

Lawrence Berkeley National Laboratory

Recent Work

Title

THE EFFECT OF ANGULAR MOMENTUM ON FISSION PROBABILITY

Permalink

<https://escholarship.org/uc/item/79c816r3>

Author

Gilmore, John.

Publication Date

1960-07-01

UNIVERSITY OF
CALIFORNIA

Ernest O. Lawrence

*Radiation
Laboratory*

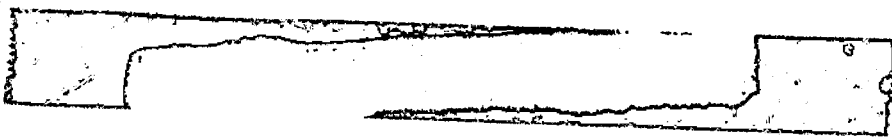
THE EFFECT OF ANGULAR MOMENTUM
ON FISSION PROBABILITY

TWO-WEEK LOAN COPY

*This is a Library Circulating Copy
which may be borrowed for two weeks.
For a personal retention copy, call
Tech. Info. Division, Ext. 5545*

DISCLAIMER

This document was prepared as an account of work sponsored by the United States Government. While this document is believed to contain correct information, neither the United States Government nor any agency thereof, nor the Regents of the University of California, nor any of their employees, makes any warranty, express or implied, or assumes any legal responsibility for the accuracy, completeness, or usefulness of any information, apparatus, product, or process disclosed, or represents that its use would not infringe privately owned rights. Reference herein to any specific commercial product, process, or service by its trade name, trademark, manufacturer, or otherwise, does not necessarily constitute or imply its endorsement, recommendation, or favoring by the United States Government or any agency thereof, or the Regents of the University of California. The views and opinions of authors expressed herein do not necessarily state or reflect those of the United States Government or any agency thereof or the Regents of the University of California.



UCRL-9304

UC-4 Chemistry General
TID-4500 (15th Ed.)

UNIVERSITY OF CALIFORNIA

Lawrence Radiation Laboratory
Berkeley, California

Contract No. W-7405-eng-48

THE EFFECT OF ANGULAR MOMENTUM
ON FISSION PROBABILITY

John Gilmore
(Thesis)

July 1960

Printed in USA. Price \$2.00. Available from the
Office of Technical Services
U. S. Department of Commerce
Washington 25, D.C.

THE EFFECT OF ANGULAR MOMENTUM
ON FISSION PROBABILITY

Contents

Abstract	3
I. Introduction.....	4
II. Experimental Procedures	
A. Fission Chamber.....	8
B. Fission Chamber Geometry.....	10
C. Target Preparation.....	17
D. Emulsions and Development.....	18
E. Scanning Procedure	23
F. Beam Integration	26
G. Beam Energy Measurement	29
III. Determination of Fission Cross Sections.....	34
IV. Calculation of Compound-Nucleus Cross Sections, Angular Momenta, and Excitation Energies	
A. Compound-Nucleus Cross Sections.....	41
B. Angular Momentum.....	41
C. Excitation Energy.....	55
V. Results and Discussion	
A. Fission Probability as a Function of Excitation Energy	60
B. Correlation of Fission Probability and Angular Momentum	60
C. Factors Affecting Compound Nucleus Formation and Angular Momentum.....	76
Acknowledgements	81
References.....	82

THE EFFECT OF ANGULAR MOMENTUM
ON FISSION PROBABILITY

John Gilmore

Lawrence Radiation Laboratory and Department of Chemistry
University of California, Berkeley, California

July, 1960

ABSTRACT

A nuclear emulsion technique has been used to determine total fission cross sections in the following heavy-ion bombardments: ($C^{12} + Tm^{169}; O^{16} + Ho^{165}$), ($O^{16} + Tm^{169}; Ne^{20} + Ho^{165}$), ($C^{12} + Re^{185}; O^{16} + Ta^{181}$), ($O^{16} + Re^{185}; Ne^{20} + Ta^{181}$). Each pair of bombardments resulted in the same compound nucleus, and excitation energies could be made equal in the two cases by adjustment of bombarding energies.

The ratio of the fission cross section to a calculated compound nucleus formation cross section, σ_f/σ_c , was taken as a measure of fission probability in each bombardment. In most bombardments a larger value of σ_f/σ_c for the heavier ion was associated with a higher angular momentum brought in by that ion. This correlation supported liquid-drop-model calculations which predict that fission should be enhanced because of an effect of angular momentum in lowering the fission barrier. Indirect effects of angular momentum on fission probability through hindrance of neutron and charged-particle emission were taken into account.

Values of σ_f/σ_c in the bombardments with full energy Ne^{20} ions were unexpectedly low. This observation led to consideration of the possibility, suggested by liquid drop calculations, that compound nucleus formation would be forbidden for very large angular momenta.

The effects of including polarization and target nucleus deformation in calculations of σ_c and angular momentum were discussed briefly.

THE EFFECT OF ANGULAR MOMENTUM ON FISSION PROBABILITY

John Gilmore

Lawrence Radiation Laboratory and Department of Chemistry
University of California, Berkeley, California

July 1960

I. INTRODUCTION

An examination of the effect of angular momentum in fission as well as other nuclear reactions has been stimulated by the increasing availability of heavy-ion accelerators. Because of its large mass, a heavy ion such as C^{12} can contribute a substantial amount of angular momentum ($> 50 \hbar$) to a reaction, even when the velocity of the ion is low enough to ensure a high probability for compound nucleus formation.

It has been observed that for heavy-ion bombardments of elements as light as rhenium and gold, fission accounts for a significant portion of the total reaction cross section. In one of the first studies of heavy-ion-induced fission, Miller, in 1952, bombarded bismuth loaded emulsions with 126-Mev C^{13} ions.¹ In this case an appreciable fission cross section was expected to result, for two reasons. The initial compound nucleus $^{222}_{89}Ac$ had a relatively high atomic number and a deficiency of neutrons -- both factors which tend to lower the fission barrier. In addition, a large amount of excitation energy in the compound nucleus made possible the evaporation of several neutrons, with further lowering of the fission barrier. In agreement with expectation, the fission cross section was found to equal approximately 50% of the total reaction cross section.

The results of bombardments of Au^{197} with N^{14} ions ($E_{max} = 125$ Mev, $E_{mean} = 60$ Mev) were reported by Fremlin in 1956.² Radiochemical determinations of fission and other reaction products led to the conclusion that comparable numbers of compound nuclei fissioned and de-excited by neutron emission.

The examination of fissionability in heavy-ion bombardments was extended to a still lighter element when Druin, Polikanov, and Flerov

bombarded Re^{185,187} as well as Au¹⁹⁷, Bi²⁰⁹, U²³⁵, and U²³⁸ with N¹⁴ ions.³ They used an ionization chamber to determine fission cross sections as a function of bombarding energy. For the rhenium target, bombardment with 80-Mev N¹⁴ ions resulted in a fission cross section of 50 millibarns, with a factor of ten increase as the ion energy was increased to 100 Mev. Halpern observes that the Re + N fission cross section at 80 Mev represents 10% of the cross section for formation of the compound nucleus Pb¹⁹⁹.⁴ He compares this figure with a fission-to-total-cross-section ratio of only 3×10^{-3} for the bombardment of lead with neutrons⁵ to give a similar excitation energy. Part of this discrepancy may be explained by the fact that bombardment of lead isotopes with neutrons gives compound nuclei with more neutrons and higher fission barriers than compound nuclei from the Re + N bombardment. Halpern suggests, however, that the larger angular momentum in the N¹⁴ bombardment may also enhance fissionability in that case. He examines a possible relation between angular momentum and fission probability by considering effects of angular momentum on factors in a simple expression for the ratio of fission to neutron level widths:

$$\Gamma_f/\Gamma_n = N \exp [(B_n - B_f)/T]. \quad (I - 1)$$

Here B_n is the neutron binding energy, B_f the fission barrier, T the nuclear temperature, and N a factor with a weak dependence on excitation energy. If the nucleus possesses an angular momentum ℓ , part of the excitation energy is in the form of rotational energy $\hbar^2 \ell^2 / 2J$, where J is the rigid body moment of inertia. Since the transfer of excitation into rotational energy results in a decrease in the density of states in a final nucleus, the process of neutron emission is effectively hindered. Halpern expresses the "unavailability" of rotational energy in neutron emission by adding the term $\hbar^2 \ell^2 / 2J$ to the neutron binding energy, B_n . In a similar sense, Halpern suggests that an amount of excitation in the form of a rotational energy term $\hbar^2 \ell^2 / 2J_s$, is unavailable for fission and should be added to the fission barrier. In this case, J_s is the moment of inertia at the saddle point about an axis perpendicular to the fission direction. Since J_s is greater than J , the term $B_n - B_f$ in expression (I - 1) is increased by a net

amount $\frac{h^2 \ell^2}{2} \left(\frac{1}{J} - \frac{1}{J_s} \right)$ and the competition of fission over neutron emission is enhanced.

As a test of this interpretation, Halpern estimates the increase in Γ_f/Γ_n for uranium isotopes formed in the $(\alpha, 4n)$ reaction relative to the same isotopes undergoing photofission. In the former case, the angular momentum deposit is considerably larger and Γ_f/Γ_n is predicted to be 1.5 times the photofission value. Experimentally, Γ_f/Γ_n for the higher angular momentum system is found to be larger by a factor of two.

An alternative point of view of the angular momentum effect is taken in a 1958 paper by Pik-Pichak.⁶ Using the liquid-drop model, Pik-Pichak evaluates the sum of changes in surface, Coulomb, and rotational energies as a function of deformation for a fixed angular momentum. The fission barrier was found to decrease with increasing angular momentum, eventually going to zero for angular momentum equal to a critical value. Pik-Pichak's expression for the fission barrier is

$$B_f = 4\pi R^2_0 \left[0.73 z^3 - (1.2z + 5.6z^2)y + (4.6 + 11z)y^2 \right], \quad (I - 2)$$

where

$$4\pi R^2_0 = \text{surface energy of undistorted drop}$$

$$= 15 A^{2/3} \text{ Mev,}$$

$$z = 1 - x = 1 - \frac{Z^2}{A} / \left(\frac{Z^2}{A} \right)_{\text{crit}}$$

$$y = \frac{\ell^2/2J_{\text{sphere}}}{4\pi R^2_0}$$

Expression (I-2) is intended to apply to nuclei with large x values, i. e., nuclei for which the saddle point configuration is close to spherical.

Hiskes has observed⁷ that expression (I - 2) gives the difference in energy between the saddle point configuration and the rotating sphere. He points out that the ground state configuration should be the

equilibrium configuration of a rotating ellipsoid rather than the rotating sphere. For that case, Hiskes gives the fission barrier equation,

$$B_f = 4\pi R^2_0 \left[\frac{49}{135} z^3 - \frac{7}{3} zy + \left(\frac{2}{3} y + \frac{14}{45} z^2 \right) \left(\frac{49}{36} z^2 + \frac{35}{12} y \right)^{1/2} \right]. \quad (I - 3)$$

In addition, Hiskes has initiated a program to calculate equilibrium and saddle-point configurations and energies for low values of x , using a variation-iteration technique in conjunction with the IBM 704 computer.

One may note a fundamental difference between the views of Halpern and those of Pik-Pichak and Hiskes. Halpern appears to consider that angular momentum effectively raises the fission barrier, while the latter authors find that a lowering of the barrier results. It would seem reasonable that rotation may be considered to lower the barrier, as found by Pik-Pichak and Hiskes, but that when one is defining the excitation energy of the nucleus at the saddle point, the rotational and deformation energies should be considered as unavailable.

The object of this work was to determine the nature of any angular momentum effect on probability for heavy-ion-induced fission. It was found possible to select pairs of isotopes that could be bombarded with two different heavy ions to give the same compound nucleus. The excitation energies in the two compound nuclei could be made equal by adjustment of the bombarding energies, but the angular momentum brought in by the heavier ion was in general greater because of its larger mass and radius. It was then of interest to find whether, in bombardment by the heavier ion, the higher angular momentum might result in an increased fission probability. Here the fission probability was defined as the ratio of the fission cross section to that for compound-nucleus formation. Compound-nucleus-formation cross sections were calculated quantities whereas the experimental portion of this work consisted of determination of fission cross sections.

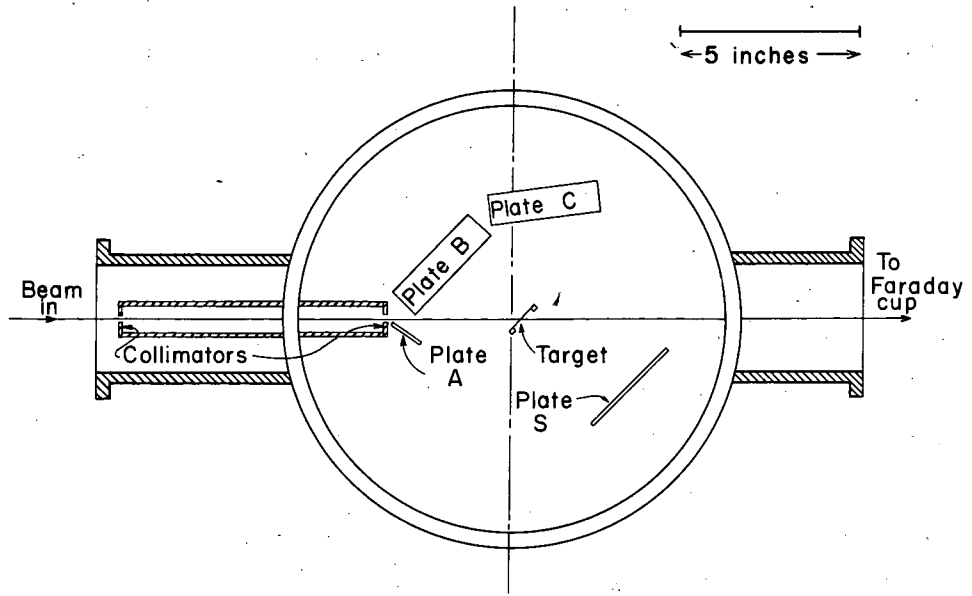
II. EXPERIMENTAL PROCEDURES

A. Fission Chamber.

A diagram of the fission chamber is shown in Fig. 1. Upon emerging from the final accelerating section of the Hilac, the heavy ions passed through an analyzing magnet and were deflected through an angle of 15 deg before entering the chamber. Magnetic analysis of the beam was found necessary; spectra of the beam taken without deflection indicated the presence of substantial amounts of low energy components. After collimation, the beam passed through a thin target and entered a Faraday cup attached to the rear of the fission chamber.

The chamber was designed by Dr. Eugene Goldberg and Dr. Harry L. Reynolds and used by them for experiments in elastic scattering^{8,9} and fission-fragment angular distributions. The interior of the chamber was modified for this work so that emulsions recorded fission fragments leaving the target at angles of from 60 to 178 deg with respect to the beam direction. Subject to the assumption that a fission-fragment angular distribution is symmetric about 90 deg in the center-of-mass system, we may confine observations to the backward hemisphere in that system. This was done in the present experiment with the result that the possibility of confusing fission-fragment tracks with scattered heavy ions and forward-directed reaction products was considerably reduced. (The presence of nickel target backings would, in any case, have complicated simultaneous observation of forward and backward recoiling fission fragments.) In order to improve recognition of fission fragment tracks, emulsions were inclined so that fragments entered the plate at angles of not more than 30 deg to the surface.

Emulsion holders, target holder, and collimators were fixed to the base of the chamber. Collimation was accomplished by 1/8-inch-diameter circular apertures fixed 7.5 inches apart. The beam profile at the target position was checked each time the chamber was set up by placing a disc of Ozalid paper in the target holder and passing approximately 0.1 millimicroampere-hour of beam through the chamber. A scorched area or "burn pattern" resulted, defining the beam profile.



MU-19346

Fig. 1. Fission chamber.

It was found desirable to locate absorber foils used for beam energy degradation as close as possible to the front collimator in order to minimize loss of beam through scattering in the foils. Accordingly, an absorber holder was mounted on the forward side of the first collimator. Absorbers were cut from aluminum foils and their thicknesses determined by weighing sections of known area.

B. Fission-Chamber Geometry.

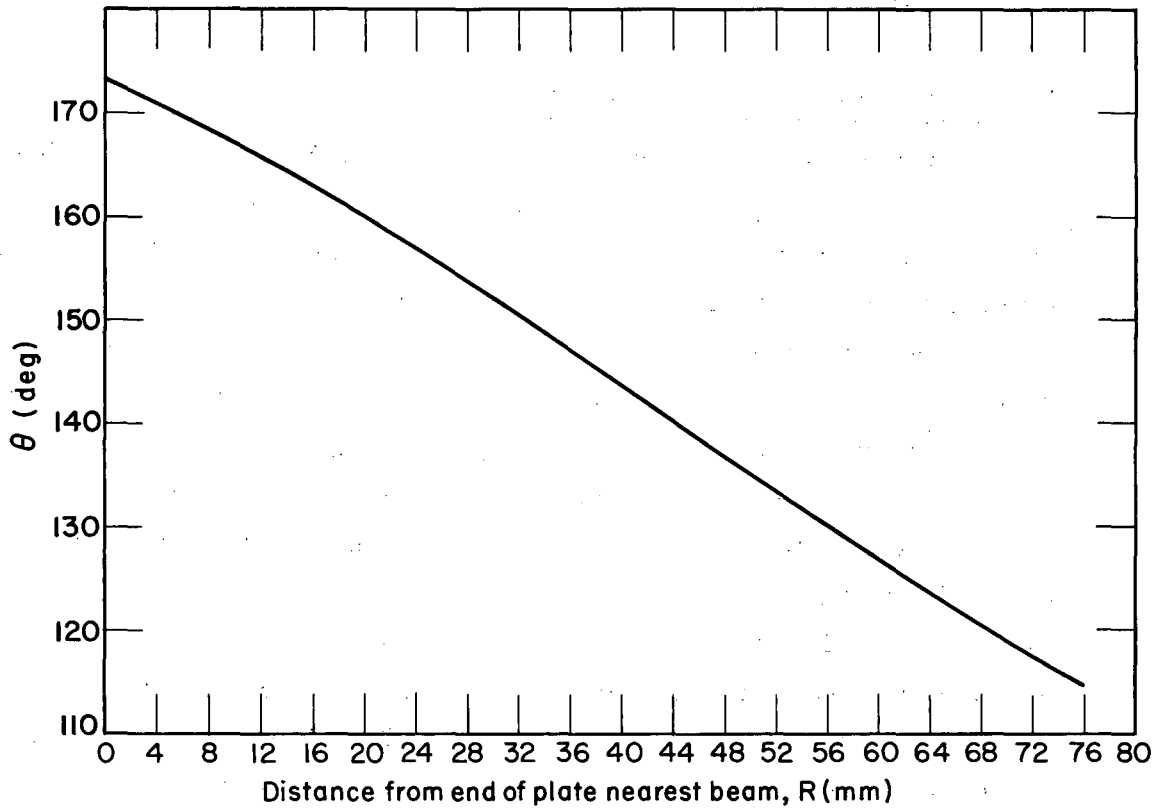
Curves (Figs. 2 and 3) giving the angle θ of recoiling fragments with respect to beam direction as a function of distance along the plate were computed from measurements of the chamber. The error in θ arising from error in geometry measurements was estimated as ± 0.5 deg.

Isogonal maps (Fig. 4) of Plates B and C were determined graphically and used to find the angular interval of observation as a function of area scanned and of θ . For the area normally scanned (0.5 mm wide and 3 mm to either side of the long axis of the plate) the angular interval of observation was found to reach a maximum of 2.2 deg at the low angle end of Plate C.

Other factors contributing to a loss in angular resolution in the use of the fission chamber have been discussed by Goldberg and Reynolds.⁸ Finite collimator size and scattering in the target were considered and found to lead to a half width in angular resolution of approximately 3 deg.

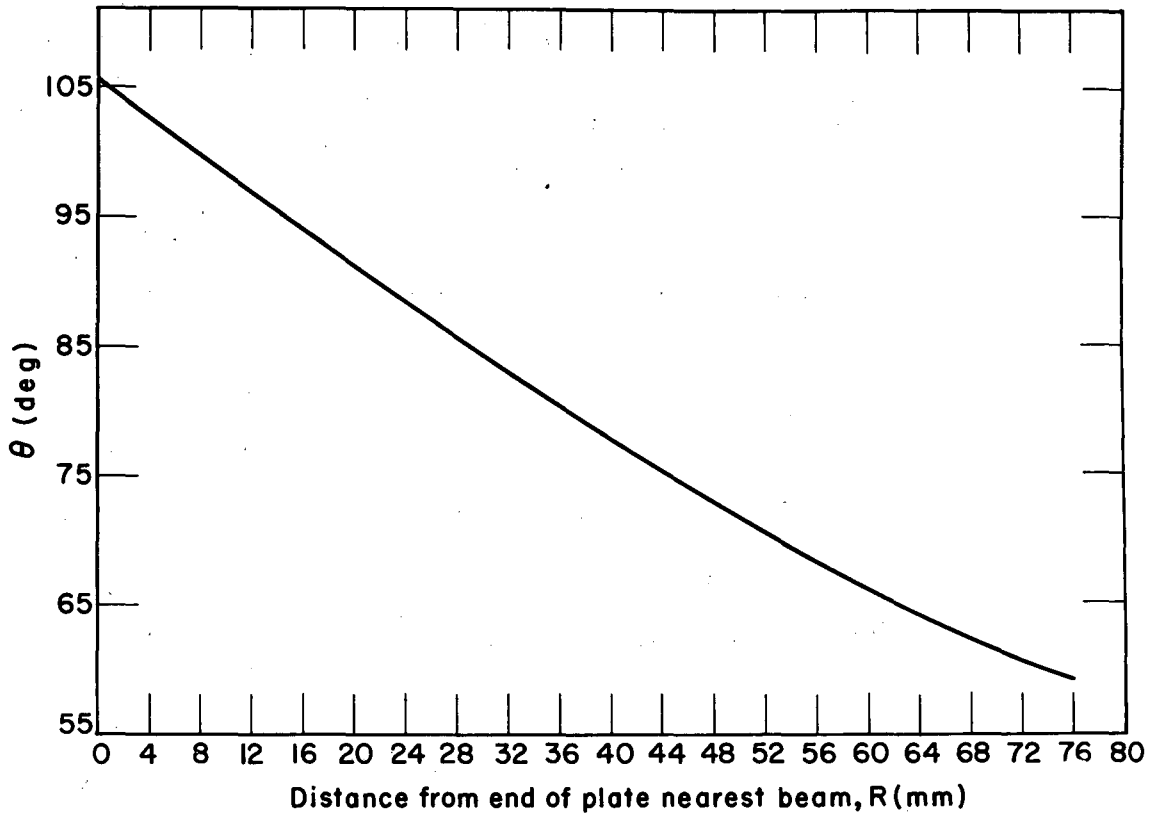
A factor T (Figs. 5 and 6) was computed from chamber measurements and used to relate an area scanned to the solid angle intercepted in the laboratory system. T is a function of the distance from target to observed area, of the slope of the plate, and of θ , and is numerically equal to the fraction of the total solid angle about the target represented by an area of 1 mm^2 at the plate center line.

The calculated geometry correction factors were checked by applying them to observations made with an alpha particle source of known intensity placed at the target position. A $64038 \pm 57 \text{ cpm Th}^{230}$ source of approximately the same area as the collimated beam was placed in the chamber with alpha sensitive emulsions and an exposure of 10.12 hours carried out. Observations of the number of tracks found in an area of 2.92 mm^2 are plotted as closed circles versus θ in Fig. 7. The observed numbers of tracks after division by $2.92 T$ are shown as open



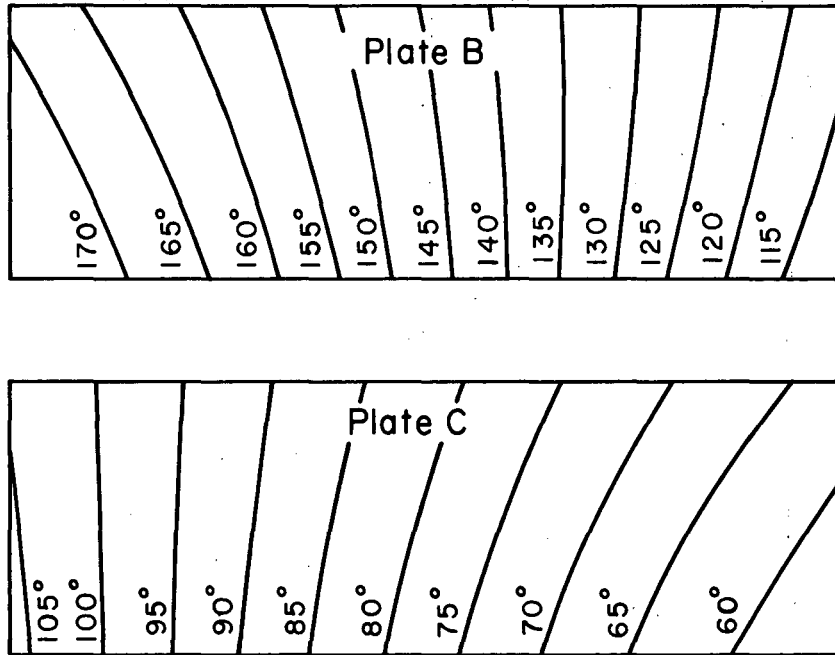
MU-21011

Fig. 2. Angle of recoil vs distance along Plate B.



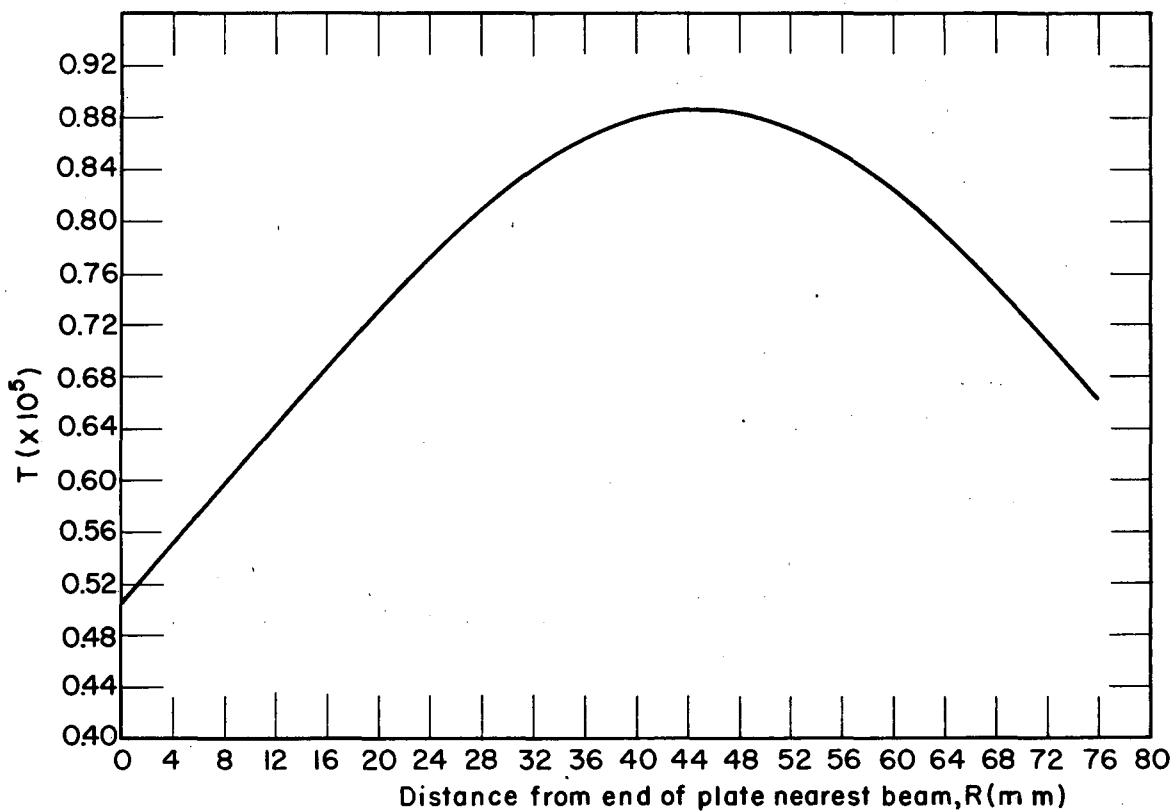
MU-21012

Fig. 3. Angle of recoil vs distance along Plate C.



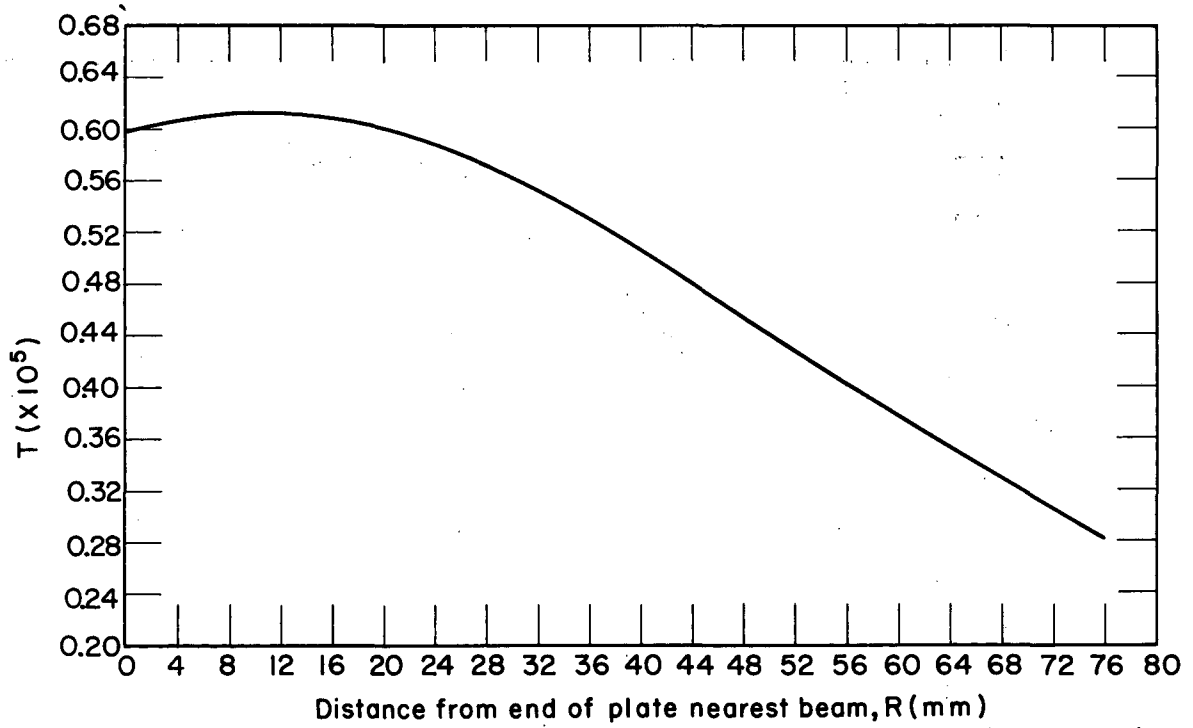
MU - 21013

Fig. 4. Isogonal maps of Plates B and C.



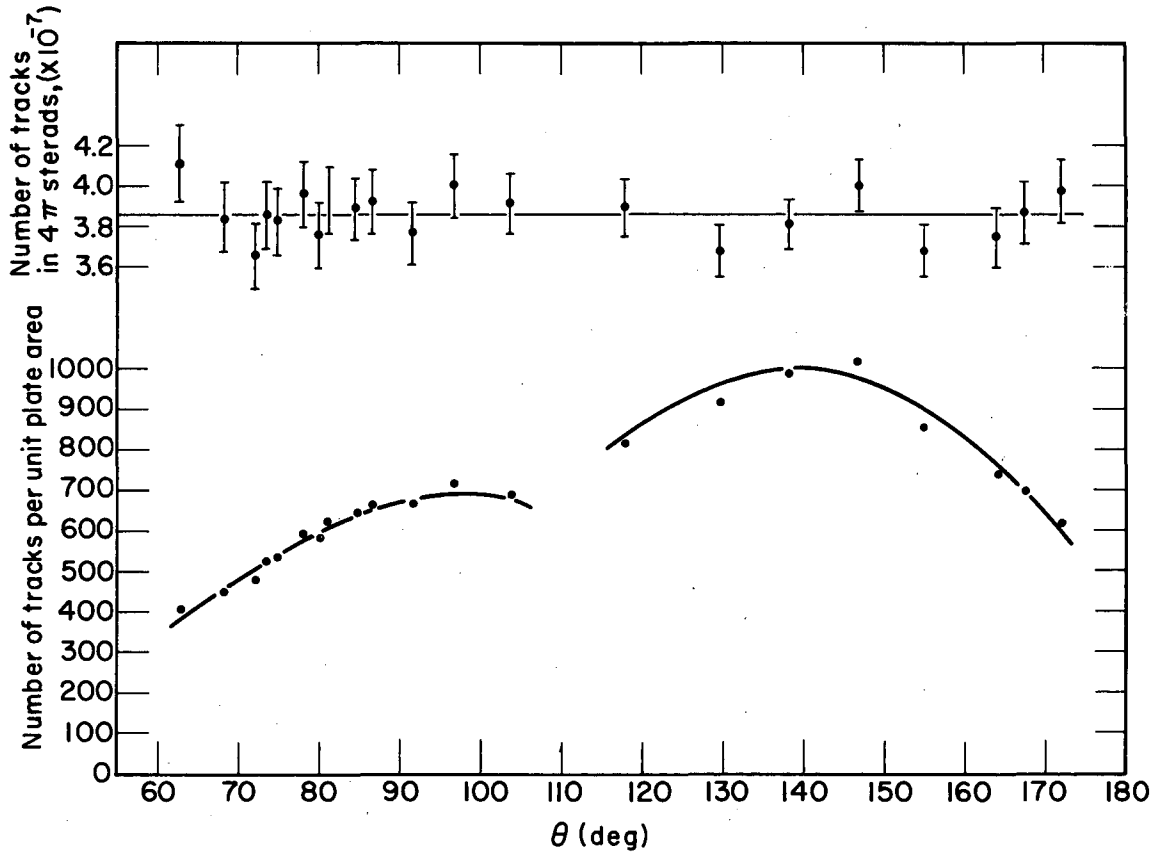
MU-21014

Fig. 5. Solid-angle correction factor vs distance along Plate B.



MU-21015

Fig. 6. Solid-angle correction factor vs distance along Plate C.



MU-21016

Fig. 7. Observations before (\bullet) and after (\circ) conversion to the intercepted solid angle.

circles. Within limits of expected standard deviation, the corrected observations lie along a horizontal line representing an isotropic distribution. The mean value of the corrected observations was 3.86×10^7 alpha particles emitted. Calculation of the number of alpha particles emitted based on source intensity and length of exposure gave a value of 3.89×10^7 .

C. Target Preparation.

1. Rhenium Targets.

Targets of Re^{185} and Re^{187} were prepared by electroplating the metal on 1.16 mg/cm^2 nickel backings. The separated isotopes were obtained from Oak Ridge National Laboratories. Isotopic analyses reported were, for Re^{185} : 96.0% Re^{185} , 4.0% Re^{187} ; and for Re^{187} : 98.8% Re^{187} , 1.2% Re^{185} . In neither case were heavier elements detected by spectroscopic analysis.

The electroplating procedure used was that described by Levi and Espersen.¹⁰ Plating solutions contained approx 2 mg/ml of rhenium as KReO_4 . The solutions were prepared by placing 10 to 15 mg of granular rhenium metal in a small round-bottom flask and adding approx 3 ml of 30% H_2O_2 to oxidize the metal to Re_2O_7 . The flask was heated in a boiling water bath until all the metal was in solution, and 5 ml of 0.015 N KOH was then added. The pH of the solution was adjusted to 0.9 to 1.0 with concentrated H_2SO_4 .

A plating cell was made from a 60-ml polyethylene bottle from which the bottom had been removed. The bottle was inverted, a weighed disc of nickel backing foil placed over the mouth, and the bottle cap screwed on. The inner part of the neck of the bottle was machined, and defined the area of the foil to be plated. A cathode lead, making contact with the back of the foil, was brought in through a hole drilled in the bottle cap. The anode was a platinum wire rotated by a stirring motor. Plating was carried out for approximately 40 minutes at 3.8 v and a current density of 0.2 amp/cm^2 . Under these conditions approx 0.7 mg of rhenium plated out on a circular area 1.14 cm in diameter. The plated surface appeared mirrorlike and uniform under 10x magnification. Following the plating operation, the targets were reweighed to determine surface density and spot-welded between stainless steel rings.

Original targets prepared and mounted in this manner proved sufficiently stable to be used in all bombardments.

2. Tantalum Target.

A tantalum target was prepared at UCLRL-Livermore through arrangements made by Mr. Harry Bowman. Tantalum of natural isotopic composition (99.988% Ta¹⁸¹, 0.012% Ta¹⁸⁰) was vaporized by electron bombardment onto a target backing of 1.16-mg/cm² nickel foil. The target thickness was 0.65-mg/cm² on a 1.12-cm-diameter circular area. A mounting was provided by spot-welding the target foil between stainless steel rings.

3. Holmium and Thulium Targets.

Targets of the monoisotopic elements holmium and thulium were prepared in the oxide form by Mr. Dan O'Connell. Spectrochemical analysis of the oxides failed to detect the presence of elements heavier than holmium and thulium. Upper limits for heavier elements were thus established to be: uranium less than 0.5%, thorium less than 0.5%, bismuth less than 0.05%, lead less than 0.1%.

The oxides were vaporized by electron bombardment and collimated onto 1.26-cm-diameter circular areas of 1.16-mg/cm² nickel foil. Target thicknesses were 0.538 mg/cm² Ho₂O₃ and 0.454 mg/cm² Tm₂O₃.

D. Emulsions and Development.

In early experiments with the fission chamber Ilford 50-micron-thick K. 0 emulsions were used as fission-fragment detectors. When processed with a Brussels-type development,¹¹ alpha particles, heavy ions, and fission fragments were clearly recorded. In fact, when K. 0 emulsions were exposed to heavy ions degraded to typical fission-fragment ranges, the tracks were sufficiently dense to permit confusion with fission-fragment tracks. Efforts to improve discrimination through reduction of developer concentration or development time led only to proportionate weakening of both heavy-ion and fission-fragment tracks.

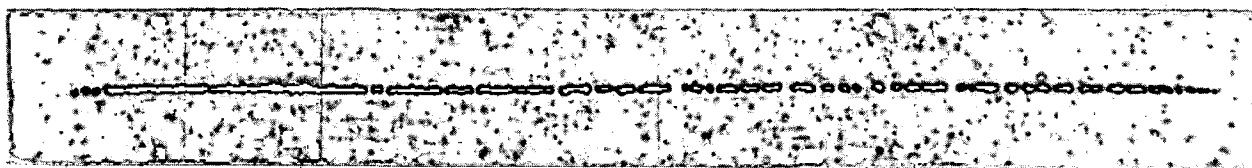
A much improved discrimination was achieved through use of

Ilford K minus 2 emulsions and a modification of a development suggested by Stevens.¹² Development of 50-micron-thick emulsions was carried out for 40 minutes at $19 \pm 1^\circ$ C in a developer of the following composition:

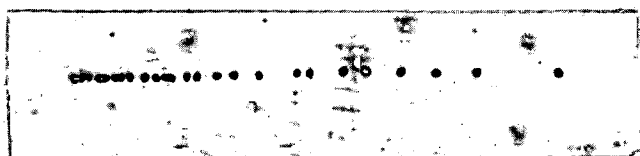
sodium phosphate (tribasic)	25	g
sodium hydrogen phosphate (dibasic)	25	g
sodium sulfite (anhydrous)	40	g
potassium bromide	4	g
sodium bisulfite	0.05	g
p-aminophenol hydrochloride	0.3	g
water -- to make	1	liter

Following development, the plates were washed for 15 minutes in tap water and fixed for at least 1/2 hour in Kodak Acid Hardening Fixer. Before drying, the plates were washed for 2 to 3 hours and soaked for 15 minutes in a 5% glycerin solution to minimize cracking of the emulsion.

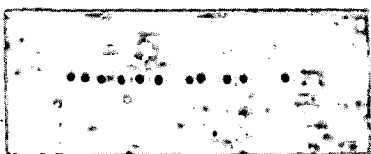
A series of K minus 2 emulsions was exposed to the different heavy ions available at the Hilac as well as to a Cf²⁵² source and processed with the foregoing procedure. Photomicrographs of the results are shown in Fig. 8. Comparison of the tracks in Fig. 8 and curves of dT/dR vs R (Fig. 9) from the work of Heckman et al.¹³ shows a correlation between grain spacing and dT/dR . For the A⁴⁰ track, the total range of the ion is recorded, but the grain spacing decreases as the end of the track is approached. In the region of maximum dT/dR the track becomes continuous but again breaks down into individual grains as the ion is neutralized and dT/dR goes to zero. For the Ne²⁰ ion only a fraction of the total range of 138 microns is recorded and the grain spacing again reflects the change of dT/dR along the track. The O¹⁶ track is recorded only as a few grains in the region of maximum dT/dR . Plates exposed to N¹⁴ and C¹² ions showed no coherent grain pattern, and the plate exposed to Cf²⁵² showed no evidence of alpha tracks. Fission tracks from Cf²⁵², on the other hand, were continuous except at the very end, where the track often broke down into one or two grains as dT/dR approached zero.



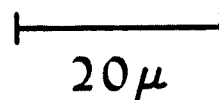
A^{40} (T=414 Mev, R=112 μ)



Ne^{20} (T=205 Mev, R=138 μ)



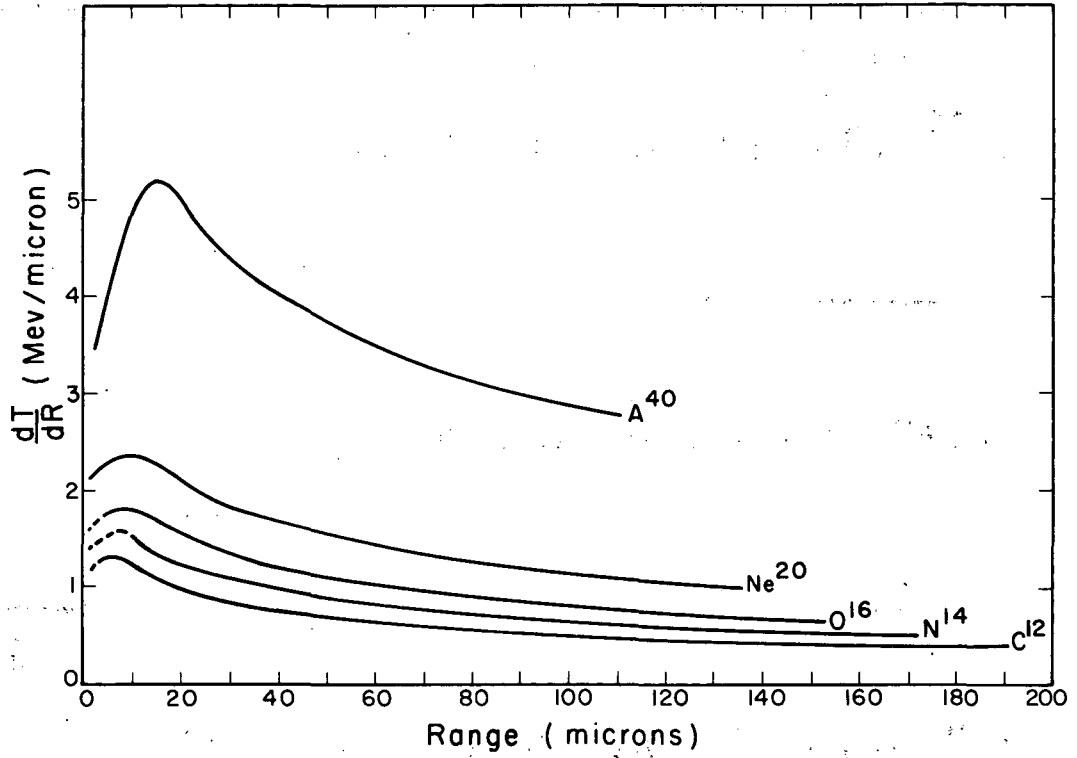
O^{16} (T=167 Mev, R=167 μ)



Cf^{252} fission fragment

ZN-2563

Fig. 8. Heavy-ion tracks in Ilford K minus 2 emulsion.



MU-17708

Fig. 9. Rate of energy loss as a function of residual range.

Comparison of Figs. 8 and 9 indicates that the combination of Ilford K minus 2 emulsion and the development described above might then be considered to possess a threshold for recording ions at approximately 1.5 Mev/micron. Since no ion heavier than Ne²⁰ was used in fission studies, this combination of emulsion and development provided adequate discrimination and was used in all subsequent bombardments.

An effect that was noticed occasionally but was not considered to introduce significant error was surface sensitization. The emulsion appeared in that case to suffer a presensitization, perhaps due to the brief exposure to a safelight while being placed in the chamber. As a result, a heavy ion which would normally be recorded as spaced grains might appear nearly continuous. However, the frequency of such tracks which also possessed a range near that of fission fragments appeared to be negligible.

In the work of Goldberg and Reynolds⁸ and in early stages of this work, a further problem arose which complicated scanning procedures. A background of developed grains at the surface of the emulsion was observed to occur with a density which increased with the total beam through the target and decreased with distance from the target to the area in question. The depth of the background was typically one to two microns, and was often dense enough to make detection of shallow tracks impossible. Although this background could be removed by rubbing the emulsion with cotton moistened with alcohol, the danger existed that fission tracks entering the plate obliquely would be removed.

A first attempt to learn the cause of the blackening consisted simply in reversing a plate so that the glass side faced the target. When no blackening occurred at the glass-emulsion interface, it was concluded that the blackening agent was not radiation in the vicinity of the visible spectrum. An alternate possibility was that the blackening was due to electrons. Although Ilford K minus 2 emulsions are far from being sufficiently sensitive to record individual electron tracks, it appeared conceivable that a high flux of electrons could create enough latent-image centers in a grain to render it developable. Such a flux of electrons quite probably arises in the form of delta rays when the heavy-ion beam passes through the target. To examine the possibility that electrons were causing the blackening, a pair of charged plates was placed between a

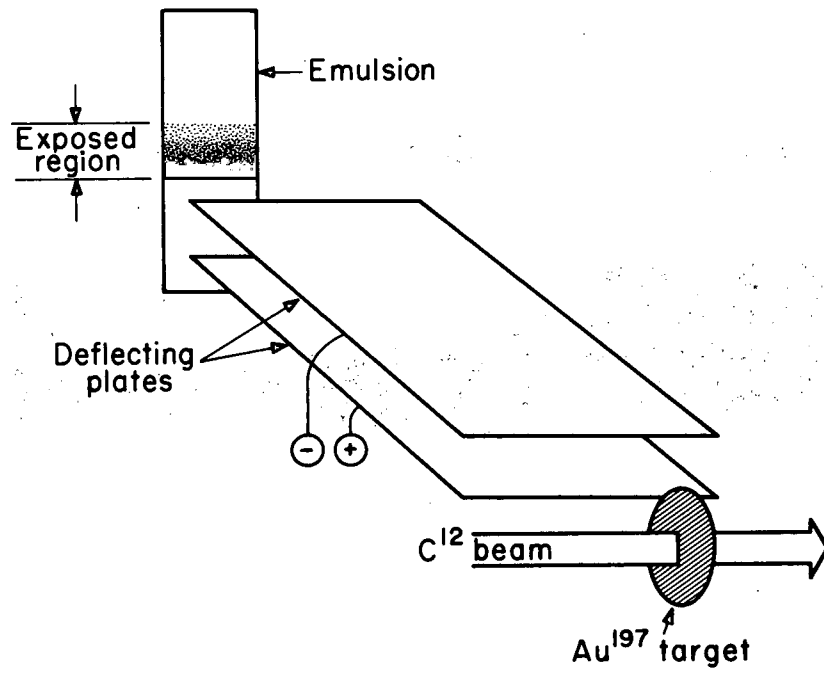
gold target and the emulsion (Fig. 10). The intensities of blackening caused by equal numbers of 124-Mev C^{12} ions through the target but with varying potentials applied across the plates are shown in Fig. 11. In Fig. 11 (b) a potential gradient of 500 v/cm has deflected a major portion of the blackening toward the bottom (positive) plate. Fig. 11 (d) shows that a potential gradient of 1500 v/cm has resulted in a substantial clearing of the emulsion.

Since the electrons were not collimated before entering the region between the plates, no very quantitative conclusions regarding the energies of the electrons could be reached from an examination of the emulsions. The following considerations show, however, that the experimental results are consistent with the blackening's being caused by delta rays. From kinetic considerations, the maximum kinetic energy of delta rays arising from passage of 124-Mev C^{12} ions through the target was calculated as 22.5 kev. The potential gradient required to deflect 22.5-kev electrons so that they would not strike the emulsion was determined to be 1180 v/cm. The reduction in blackening as this value of potential gradient was approached and exceeded suggested that the energy of the majority of electrons lay below the maximum delta ray energy.

For the purpose of preventing electrons from passing from the target to the emulsion, the magnetic field of a permanent magnet was found to be a much more efficient means of deflection than an electric field. Goldberg and Reynolds⁹ constructed a permanent magnet with pole pieces which straddled the target and provided a 1000 gauss field in the vertical direction. The radius of curvature of 22-kev electrons in this field was calculated as 0.5 cm, while the radius of a typical fission fragment was about 6 meters. The magnet of Goldberg and Reynolds⁹ was used in early stages of this work and permitted exposures to be increased by a factor of ten relative to those bombardments in which no magnet was present. In later stages of this work, a horseshoe-type magnet with a 1500 gauss field and of somewhat more convenient size was substituted.

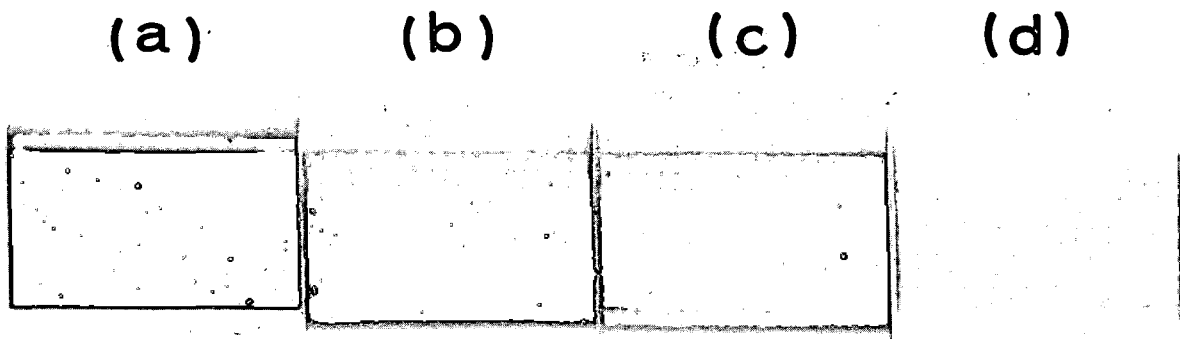
E. Scanning Procedure.

Emulsions were scanned with a Bausch and Lomb model TPR-8 binocular microscope equipped with a micrometer stage. Eyepieces were



MU-21017

Fig. 10. Electron-deflection experiment.



ZN-2564

Fig. 11. Effect of potential gradient on blackening of emulsions with positive plate at bottom. (a) 0 v/cm; (b) 500 v/cm; (c) 1000 v/cm; (d) 1500 v/cm.

Bausch and Lomb 10x wide-field type. Either a Leitz 52x or a Bausch and Lomb 98x Fluorite objective was used, depending upon the density of tracks in the area viewed.

In most cases, four adjacent scanning swaths, 3 mm to either side of and normal to the plate center line, would constitute an observation for a given angle. Such an observation, representing an area of 3.31 mm^2 , would normally be made at intervals of 5 mm along the center line and would typically include 300 fission tracks. For lower fission cross sections, proportionately more area would be scanned. When the lowest fission cross sections in this work were being determined, an area of 26.5 mm^2 was scanned at each angle.

F. Beam Integration.

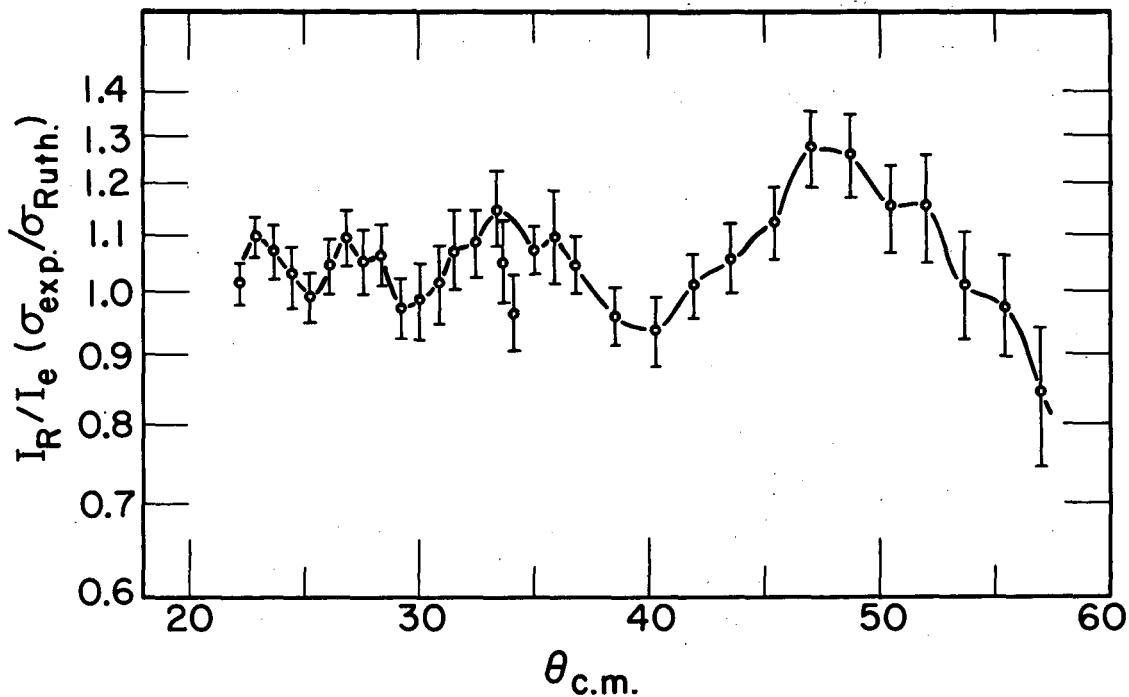
After passing through the target, the beam entered a Faraday cup where the charge was collected. Integration of the charge was performed by a 100% feedback electrometer. A large permanent quadrupole magnet straddled the mouth of the Faraday cup and helped to prevent escape of electrons from the cup. It is likely that the transverse magnetic field at the target provided by the magnet described in Section II. D. also improved the accuracy of beam integration by preventing delta rays from entering the Faraday cup.

Since the integrated beam reading entered directly into determination of fission cross sections, it was thought important to check the accuracy of integration. A comparison of experimentally determined and calculated Rutherford scattering cross sections was selected as the most convenient measure of the accuracy of beam integration. At the small scattering angles associated with large impact parameters, the scattering cross sections may be expected to agree closely with Rutherford scattering cross sections. At higher scattering angles the Blair "sharp-cutoff" model¹⁴ has been used with considerable success in describing elastic scattering of heavy ions^{8, 9, 15} and alpha particles.¹⁴ For low-angle scattering, the Blair model predicts an oscillation about unity of the ratio $\sigma_{\text{exp}}/\sigma_{\text{Ruth}}$. It predicts a rise of the ratio to 1.2 to 1.3 as the angle increases, and then a rapid drop below unity as the impact parameter becomes small enough for absorption to occur. Blair assumes that the amplitude of the outgoing ℓ th wave is zero if the distance

of closest approach is equal to or less than the sum of the radii of the two nuclei. The largest ℓ wave to be absorbed is termed ℓ' , or the cutoff ℓ value.

For the purpose of measuring scattering cross sections, a holder for Plate S was installed in the chamber (Fig. 1). This plate intercepted ions scattered at angles of from 10.63 to 56.11 deg in the laboratory system. Collimator apertures were reduced from 1/8 to 1/16 inch to improve angular resolution. Since the presence of nickel backings in all of the targets used in the fission studies prevented their use as scattering targets, a self-supporting 0.758 mg/cm² gold target was chosen. The ion used in the scattering experiment was C¹², degraded to 85.1 Mev. Two exposures of 0.100 and 0.400 millimicroampere-hours (electrometer readings) were made, to provide a convenient number of tracks per unit area in regions of both high and low scattering cross section. An area of 0.1458 mm² was scanned at each angle and converted to solid angle by using a factor similar to that described for geometry correction in the fission work (Section II. B.). From the number of ions scattered into unit solid angle and from a calculated value of the Rutherford scattering cross section, a value I_R for the total number of ions incident on the target was obtained for each observation. The ratio of this number to the number of incident ions I_e determined from the electrometer reading is plotted as a function of the center-of-mass scattering angle in Fig. 12. This ratio I_R/I_e is equal to the ratio $\sigma_{\text{exp}}/\sigma_{\text{Ruth}}$, discussed in the preceding paragraph. It may be seen that the ratio I_R/I_e exhibits the oscillatory behavior at small angles and the final rise and fall-off predicted by the Blair model. It appears, however, that the ratio oscillates about a value of approximately 1.04 rather than unity. This suggests that the electrometer reading was about 4% low. Such a difference could have been caused by delta rays entering the Faraday cup. On the other hand, the uncertainty in knowledge of target thickness, together with possible errors in determining θ and the solid angle correction factor could have contributed substantially to this 4% difference. Accordingly, no correction was applied to electrometer readings for the fission experiments.

Since the IBM 650 program which had been used⁸ to calculate the Blair value of the scattering cross section was available, it appeared



MU-21018

Fig. 12. Ratio of integrated beam current calculated from Rutherford scattering to integrated beam current measured by electrometer as a function of the center-of-mass scattering angle.

worthwhile to carry out the calculations for the system examined in this experiment. The program calculates the cross section, normalized to Rutherford scattering, as a function of $\theta_{c.m.}$ for several values of the cutoff ℓ value, ℓ' . Goldberg and Reynolds⁸ considered factors that influence oscillations in the calculation and concluded that the most important region in fitting the calculations to the data is in the vicinity of the dropoff. For this experiment the best agreement between the calculation and observations is for $\ell' = 43$. Figure 13 shows the calculation for $\ell' = 43$ plotted together with the observed values of $\sigma_{exp}/\sigma_{Ruth}$ which had been normalized by division by 1.04. By use of a value for ℓ' of 43 in the relation

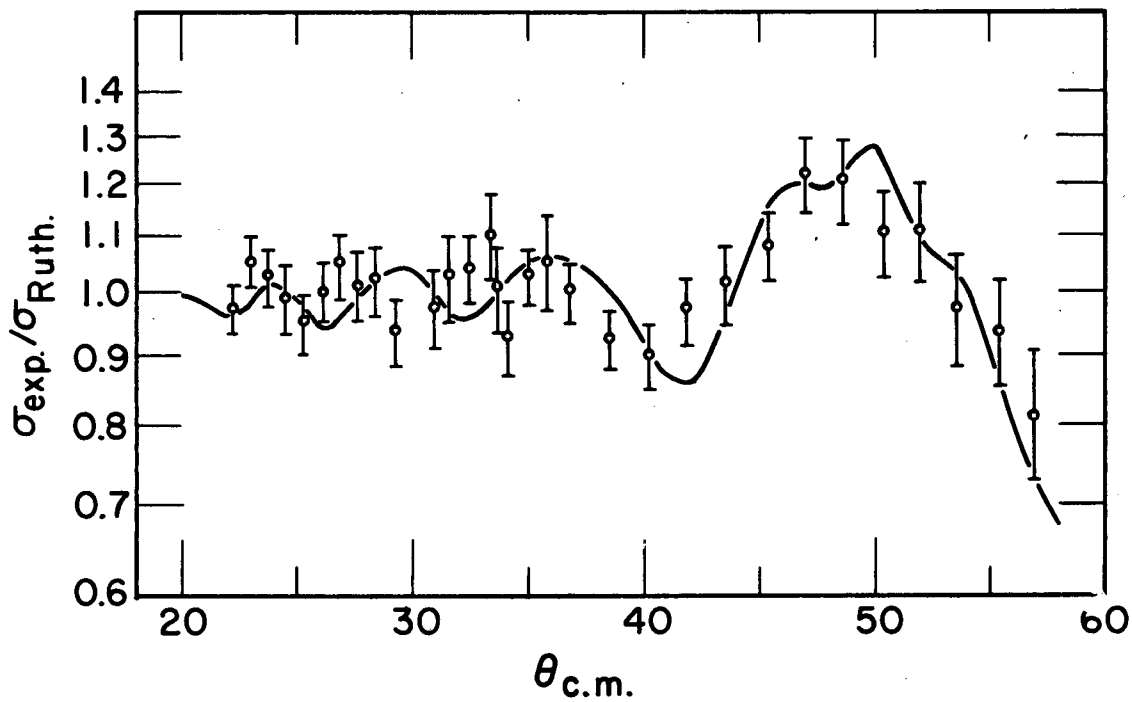
$$E_{c.m.} = \frac{Z_1 Z_2 e^2}{R} + \frac{\hbar^2 \ell'(\ell' + 1)}{2\mu R^2} \quad (II - 1)$$

a value for the interaction distance R of $12.1 \pm 0.3 \times 10^{-13}$ cm was calculated. This value is in fair agreement with Goldberg and Reynolds's value of $11.8 \pm 0.3 \times 10^{-13}$ cm for the same system.⁸ From the calculated R , a value of the radius parameter r_0 in the relation $R = r_0(A_1^{1/3} + A_2^{1/3})$ was then determined to be 1.49×10^{-13} cm.

G. Beam-Energy Measurements.

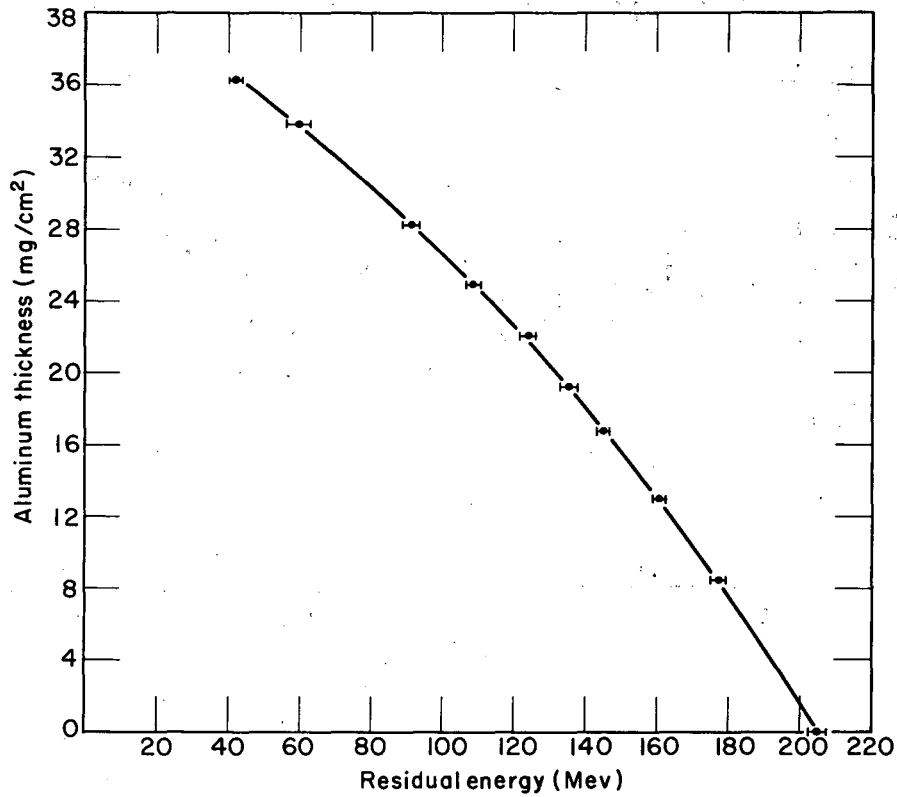
Aluminum foils were used to degrade the beams to the desired energies. Foil thickness requirements were determined from Walton's range-energy curve for C^{12} in aluminum¹⁶ and from Sikkeland's curves for N^{14} and O^{16} in aluminum.¹⁶

Range-energy data for Ne^{20} in aluminum¹⁶ were obtained during the course of this work and are listed in Table I and plotted in Fig. 14. The method of measurement had been used previously by Sikkeland¹⁷ and involved determining the residual range in emulsion of ions which had passed through a given thickness of aluminum. The residual ranges were converted to residual energies by reference to the range-energy relationships for heavy ions in emulsion of Heckman et al.¹³ For record in Ne^{20} ions, 50-micron-thick Ilford E.1 emulsions on 1 x 3 in. glass slides were used. The emulsions were inclined so that the angle between the entering ions and the plate surface was approx 5 deg. A beam current of 12 millimicroamperes (average) was reduced by a factor of



MU-21019

Fig. 13. Experimental scattering cross section normalized to Rutherford scattering cross section as a function of center-of-mass scattering angle. The solid line is the Blair model calculation for $\ell' = 43$.



MU-21020

Fig. 14. Residual energy of Ne²⁰ ions after passing through various thicknesses of aluminum.

approx 10^6 by placing two Electromesh units in the path of the beam. Under these conditions several hundred ions entered the plate in the course of a 5-minute exposure. Following the exposure the plates were developed for 10 minutes at 23° C in Kodak D-19 (1:6).

Table 1

Thickness of aluminum (mg/cm ²)	Residual energy of Ne ²⁰ (Mev)	σ (Mev)
0	205.5	1.9
8.45	177.1	2.0
12.95	160.9	1.8
16.72	145.0	1.8
19.23	135.4	2.4
22.06	124.2	2.3
24.91	108.8	2.1
28.16	91.3	2.3
33.83	59.9	3.4
36.29	42.1	1.8

Range measurements were made with the microscope described in Section II. E. , using an eyepiece reticule. One hundred tracks were measured at each energy. The true range of the ion was found from the relation

$$R(\mu) = [\rho^2 + (SZ)^2]^{1/2} - 0.46, \quad (\text{II} - 2)$$

where ρ is the projected length of the track in the plane of observation and Z is the depth of the end of the track. S is the ratio of emulsion thickness at the time of exposure to the thickness following processing. A value for S of 2.2 was determined by Torbjørn Sikkeland¹⁷ for an emulsion from the batch used for this experiment. A further correction was the subtraction of a mean grain diameter of 0.46 micron from the observed range to account for the ion's traversal, on the average, of only

one-half of the first and last grains of the track.

Since the incident energy of a given ion beam at the Hilac is observed to fluctuate by a few per cent, it was decided to measure the beam spectrum during each bombardment. For this purpose an additional emulsion holder was installed in the chamber between the second collimator and target. The emulsion holder was hinged to drop out of the way of the beam during the bombardment of a target. At the conclusion of the bombardment a permanent magnet applied to the top of the chamber drew the emulsion up into the path of the beam without requiring the chamber to be opened to the atmosphere. Emulsion type, exposure and development were the same as those used in the Ne^{20} range-energy measurements. The width of the energy distribution at half-maximum was found to be typically 2%.

III. DETERMINATION OF FISSION CROSS SECTIONS

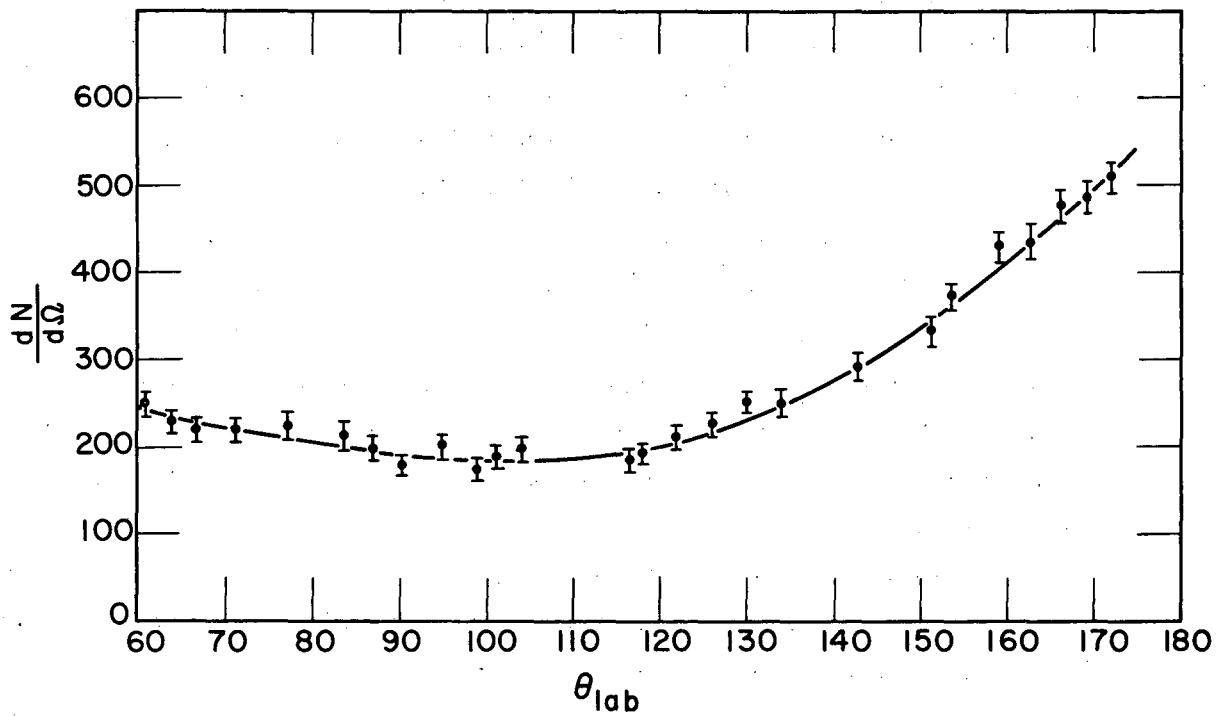
Fission cross sections were determined by integration of fission fragment angular distributions. Observations of the number of fission fragments intercepted by unit plate area were corrected for solid angle intercepted (Section II. B.) and plotted as a function of angle of recoil in the laboratory system, θ_L . An example of such a distribution is shown in Fig. 15. The distribution of Fig. 15 represents data from Plates B and C (Fig. 1) for the bombardment of Re^{185} with 79.2-Mev C^{12} ions. When converted to the center-of-mass system (Fig. 16), the distribution in Fig. 15 must be symmetric about 90 deg, provided complete fusion of the bombarding particle and target nucleus has occurred and that evaporation of neutrons or charged particles from the compound nucleus prior to fission has not altered its velocity. Such symmetry is observed in the angular distribution of fission fragments from the bombardments of Au^{197} with $\text{C}^{12,18,19,20}$ and $\text{O}^{16,21}$.

Since each observation in Fig. 15 includes a distribution of fission fragment masses and energies, the transformation to the center-of-mass (c. m.) system was made with reference to a most probable fragment mass and energy. Corresponding to the results of radiochemical studies of fragment mass distributions in fission of Au^{197} by $\text{N}^{14,22}$ and $\text{C}^{12,23}$, a division of the fissioning nucleus into equal fragments was assumed to be most probable.

The correlation by Terrell²⁴ of kinetic energy release with $Z^2/A^{1/3}$ of the fissioning nucleus was used to determine the most probable fragment kinetic energy. This correlation had previously been found to be consistent with measurements of fragment kinetic energies in the bombardment of Au^{197} with $\text{C}^{12,18}$ and $\text{O}^{16,21}$.

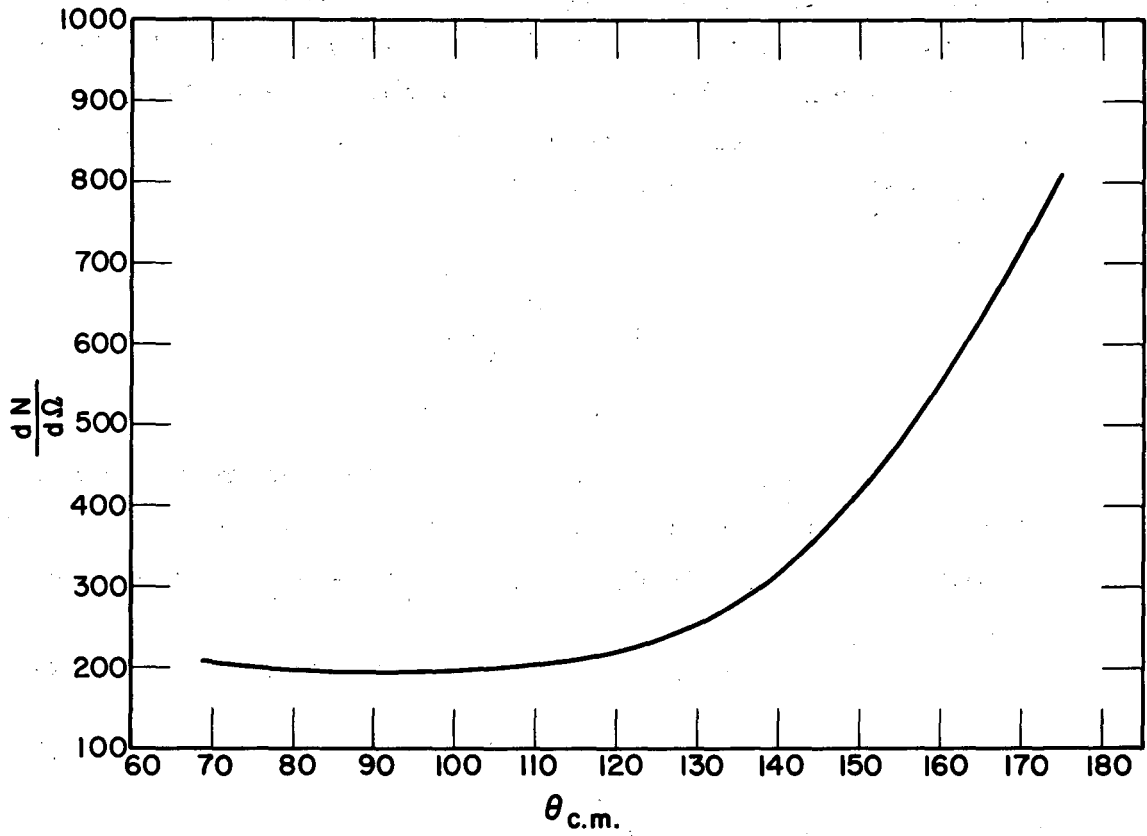
Transformations of distributions from the laboratory to the c. m. system were made with the aid of the tables of Marion, Arnette, and Owens.²⁵ In Fig. 16 it is seen that a minimum in the distribution occurs in the vicinity of 90 deg although the absence of data forward of 60 deg precludes a good test of symmetry.

The number of fission fragments entering the backward hemisphere in the c. m. system may be obtained by integrating the c. m.



MU-21021

Fig. 15. Angular distribution of fission fragments from the bombardment of Re^{185} with 79.2-Mev C^{12} ions (lab system).



MU-21022

Fig. 16. Angular distribution of fission fragments from the bombardment of Re^{185} with 79.2-Mev C^{12} ions (c. m. system).

distribution from $\pi/2$ to π or the laboratory distribution from θ_L corresponding to $\theta_{c.m.} = \pi/2$ to π . The latter procedure was followed in most of the determinations. The value of θ_L corresponding to $\theta_{c.m.} = \pi/2$ was found to be quite insensitive to the values of fragment mass and kinetic energy used in the transformation. A 20% change in fragment mass or kinetic energy resulted in a shift of approx 1.5 deg in θ_L and this change was in turn reflected in a 3% change in the number of fragments measured. Each value of $dN/d\Omega$ (Figs. 15 and 16) was multiplied by $d\Omega/d\theta = 2\pi \sin \theta$ and the resulting distribution integrated over θ to give the total number of fissions, N .

$$\theta_L = \theta_{c.m.} = \pi$$

$$N = \int_{\theta_L \rightarrow \theta_{c.m.} = \pi/2} \frac{dN}{d\theta} d\theta \quad (\text{III - 1})$$

If the angular distribution had been transformed to the c.m. system the lower limit of integration was $\pi/2$. If the laboratory system distribution was to be integrated, the lower limit was that angle corresponding to $\theta_{c.m.} = \pi/2$.

The fission cross section σ_f was calculated from the relation

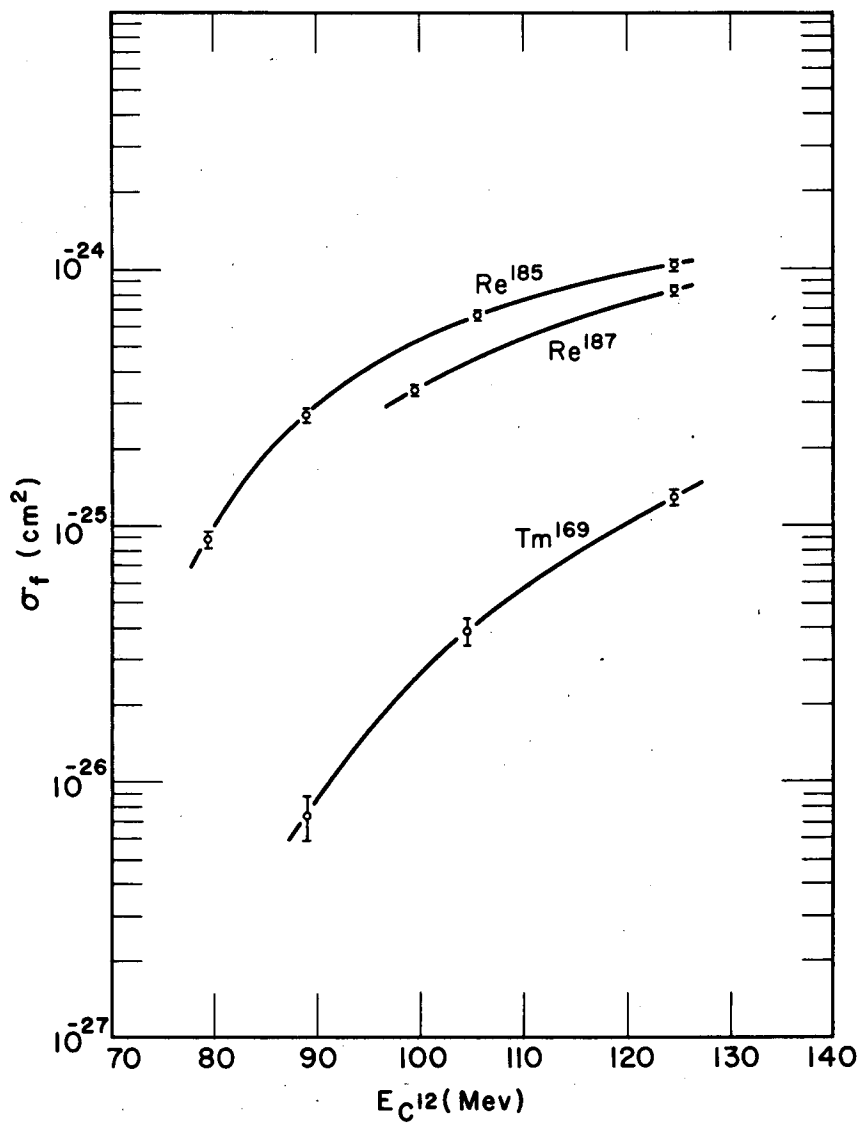
$$\sigma_f = \frac{N}{IS} \quad (\text{III - 2})$$

where N = number of fissions
 I = number of heavy ions passing through target
 S = number of target nuclei per cm^2 .

Fission cross sections are shown as a function of bombarding energy as follows:

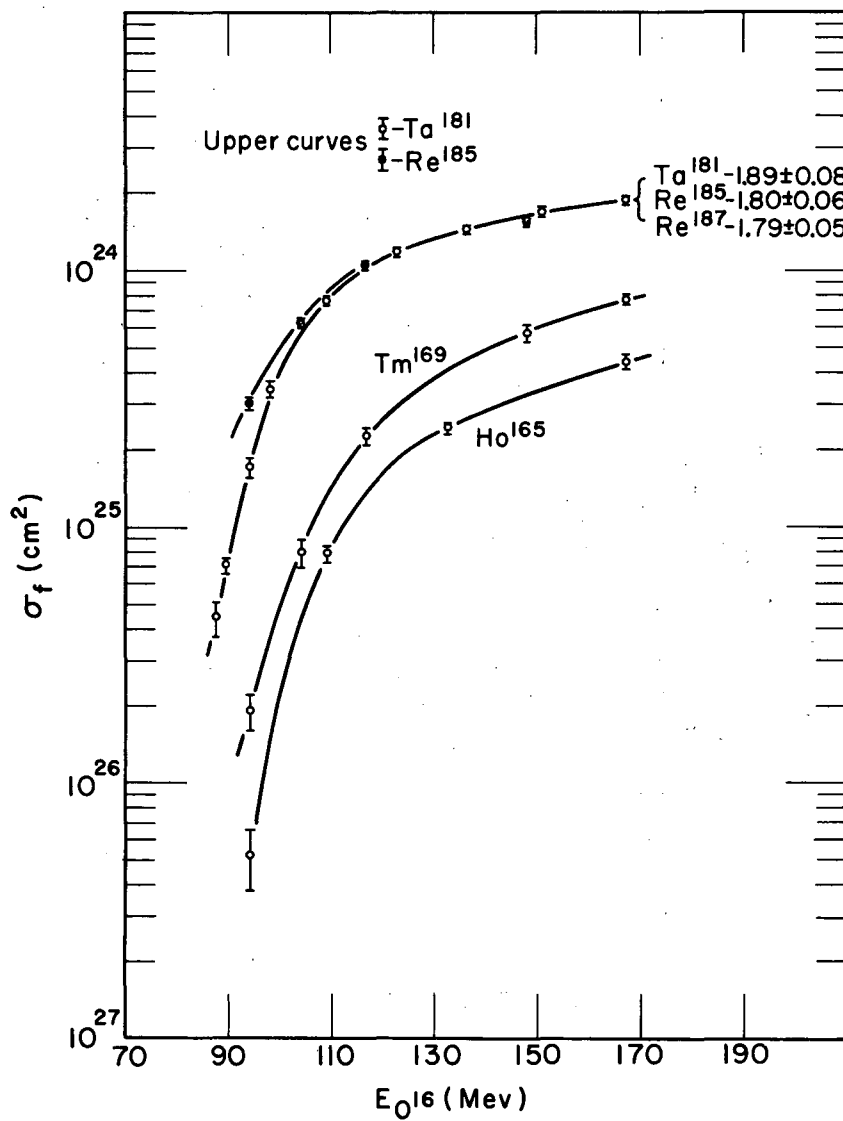
<u>Bombarding particle</u>	<u>Target nuclei</u>	<u>Fig.</u>
C^{12}	Tm^{169} , Re^{185} , Re^{187}	17
O^{16}	Ho^{165} , Tm^{169} , Ta^{181} , Re^{185} , Re^{187}	18
Ne^{20}	Ho^{165} , Ta^{181}	19

Indicated uncertainties are only those determined by counting statistics.



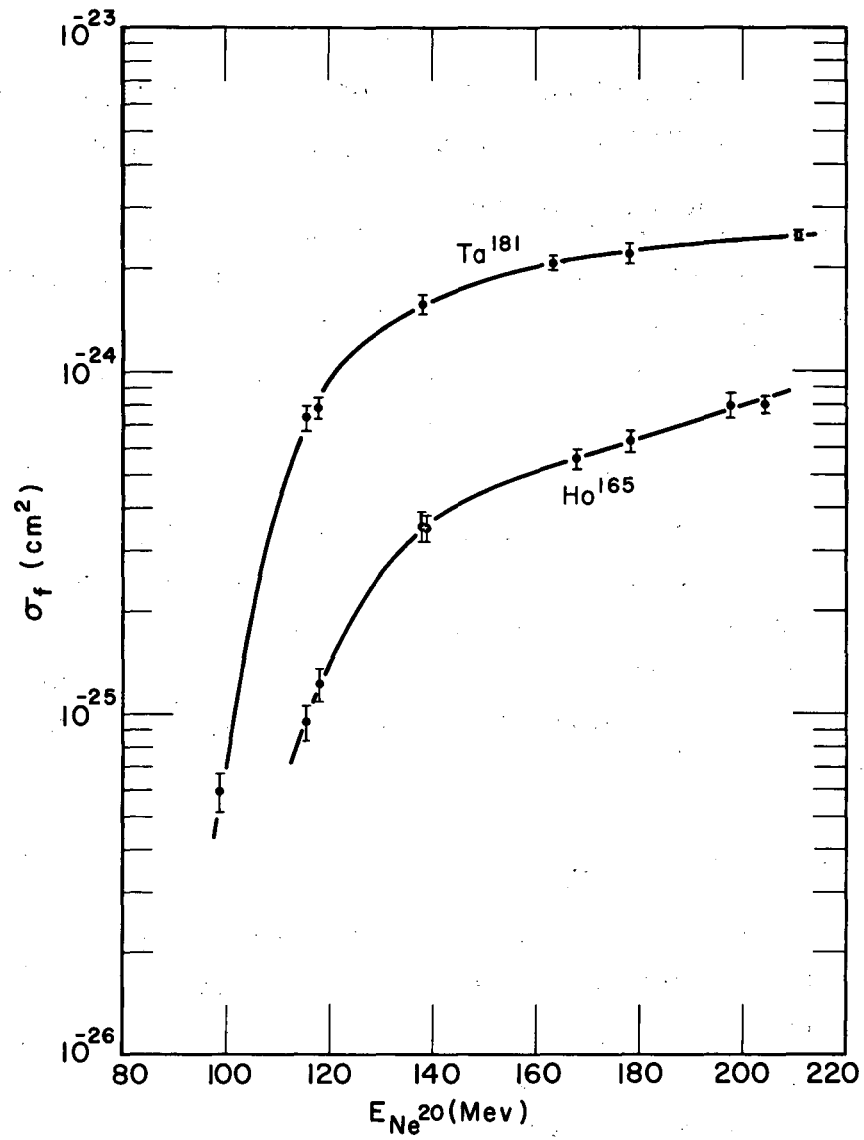
MU-21023

Fig. 17. Fission cross sections for bombardment with C^{12} ions.



MU-21024

Fig. 18. Fission cross sections for bombardment with O¹⁶ ions.



MU-21025

Fig. 19. Fission cross sections for bombardment with Ne^{20} ions.

IV. CALCULATION OF COMPOUND NUCLEUS CROSS SECTIONS, ANGULAR MOMENTA, AND EXCITATION ENERGIES

A. Compound-Nucleus Cross Sections.

Cross sections for forming compound nuclei in heavy ion bombardments were taken from the work of Thomas.²⁶ Calculations were made for square-well and diffuse-well nuclear potentials.

1. Square-Well Model.

Using assumptions from the model of Blatt and Weisskopf,²⁷ Thomas has calculated σ_c for bombardment of a number of target isotopes with several heavy ions. Values of σ_c for the systems studied in this work were obtained by interpolation in his tabulations and are shown in Figs. 20 through 27. The value of r_0 used in these calculations was 1.5×10^{-13} cm.

2. Diffuse-Well Model.

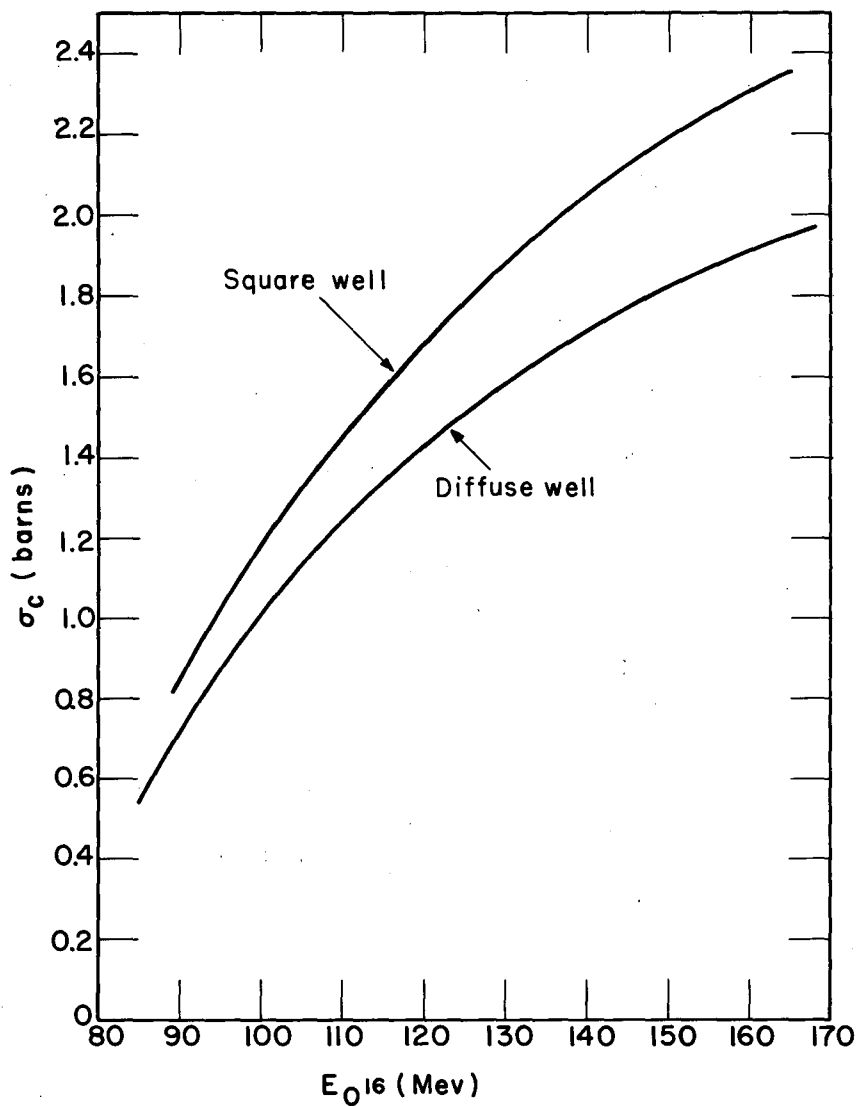
A model in which the total potential is approximated by a parabola was used by Thomas to conform with the established diffuseness of the nuclear charge distribution. The calculation was programmed for the IBM 650, using a value of r_0 of 1.17×10^{-13} cm. Values of σ_c calculated with the use of Thomas's program are shown in Figs. 20 through 27.

B. Angular Momentum.

1. Classical Calculation.

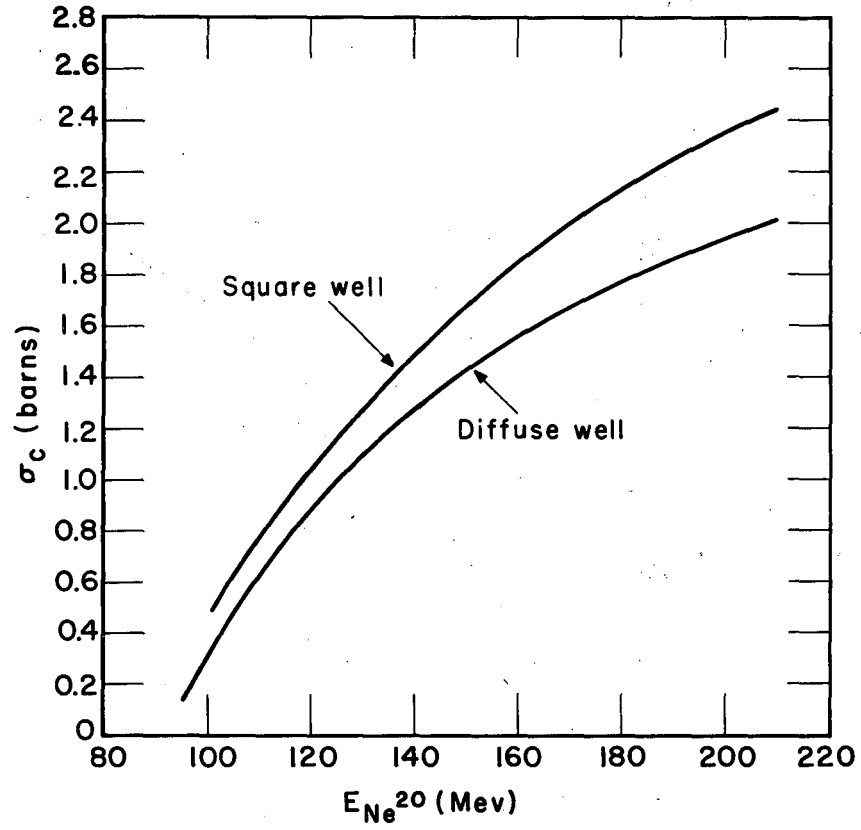
The maximum orbital angular momenta of the systems of targets and bombarding particles studied in this work were calculated* from

* In this section calculations of l_{\max} are based on spherical target nuclei. In Section V. C. 2. a calculation is discussed in which the ellipsoidal natures of the target nuclei are considered.



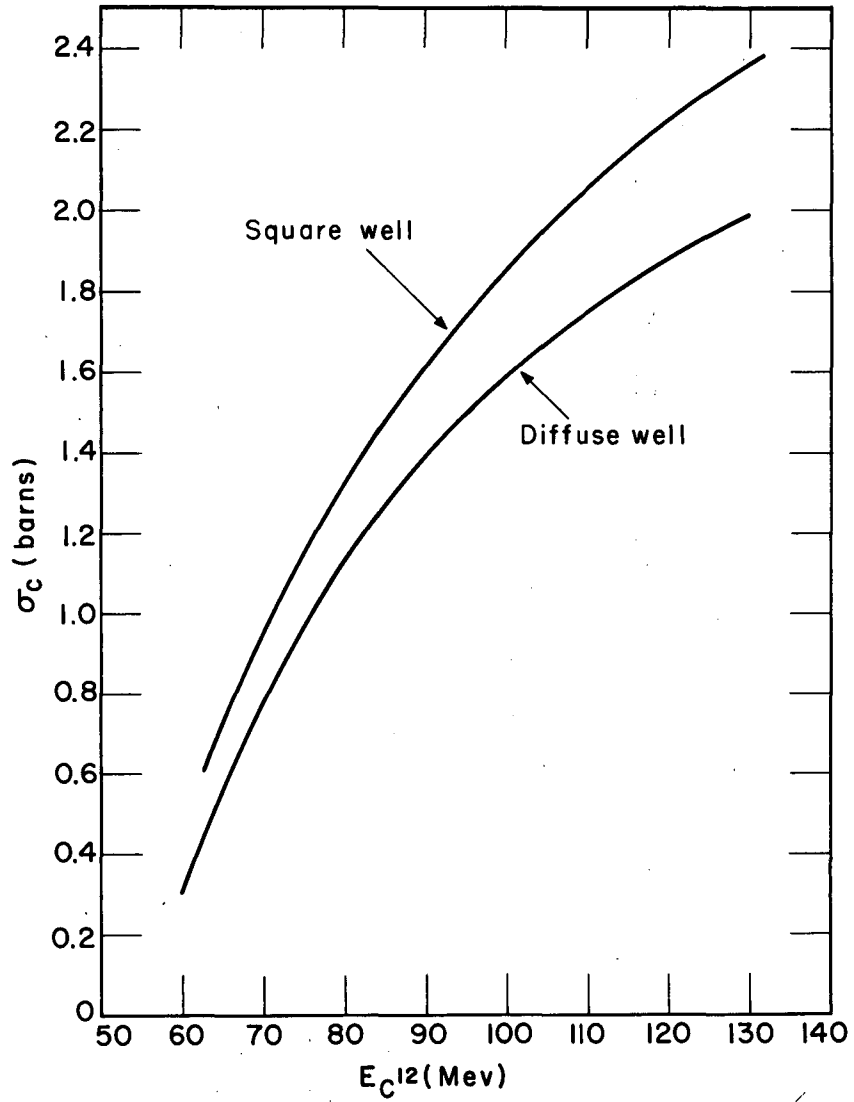
MU-21026

Fig. 20. Cross sections for compound-nucleus formation in the bombardment of Ho^{165} with O^{16} ions.



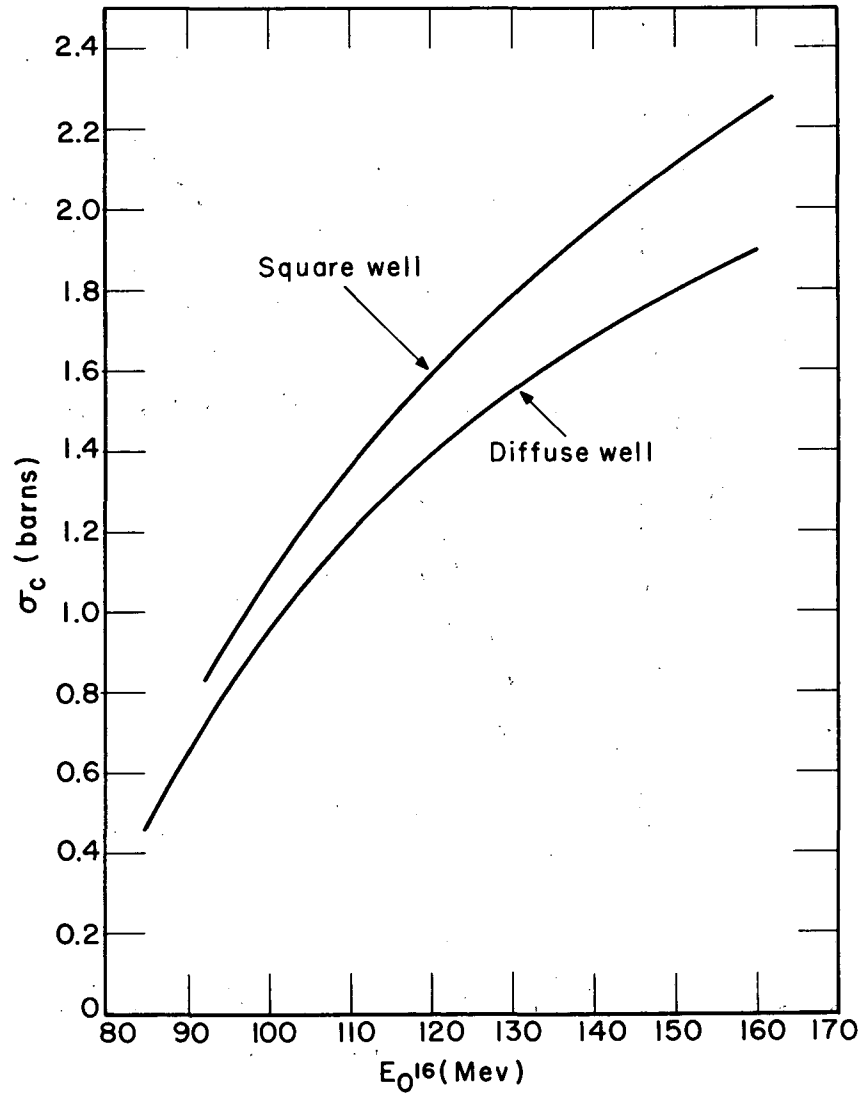
MU-21027

Fig. 21. Cross sections for compound-nucleus formation in the bombardment of Ho^{165} with Ne^{20} ions.



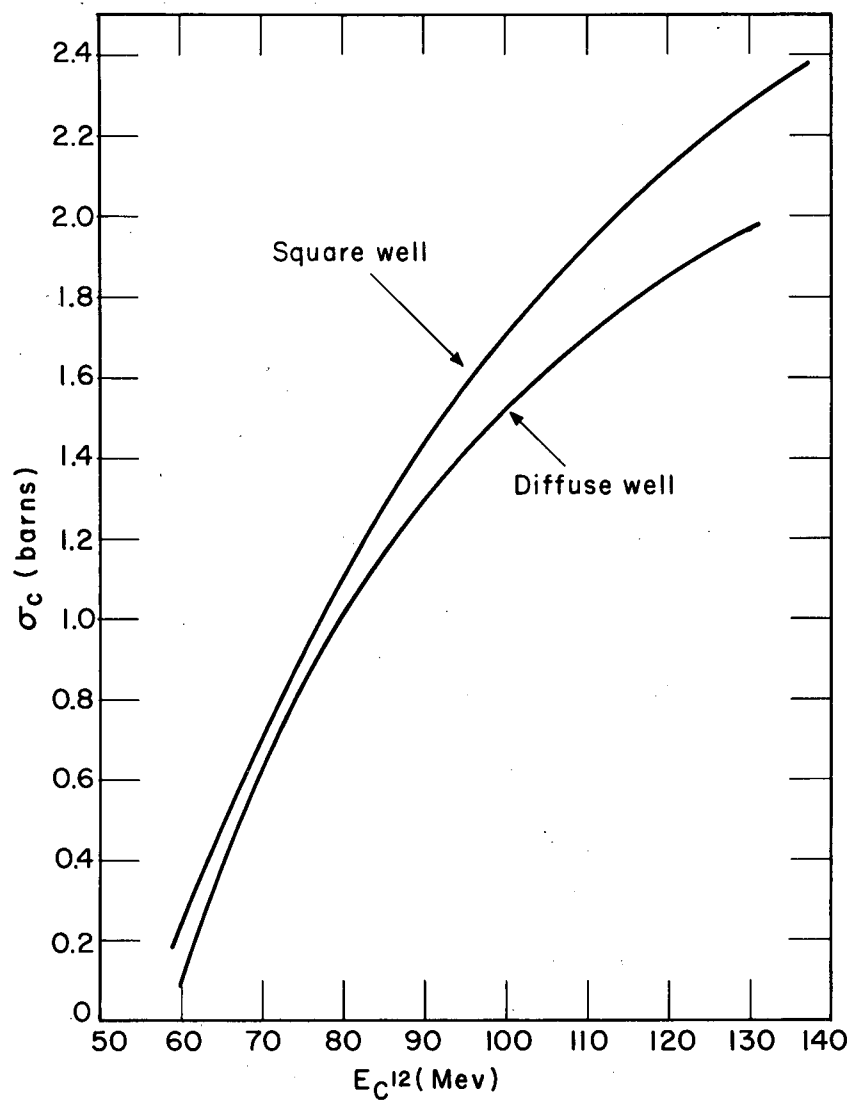
MU-21028

Fig. 22. Cross sections for compound-nucleus formation in the bombardment of Tm^{169} with C^{12} ions.



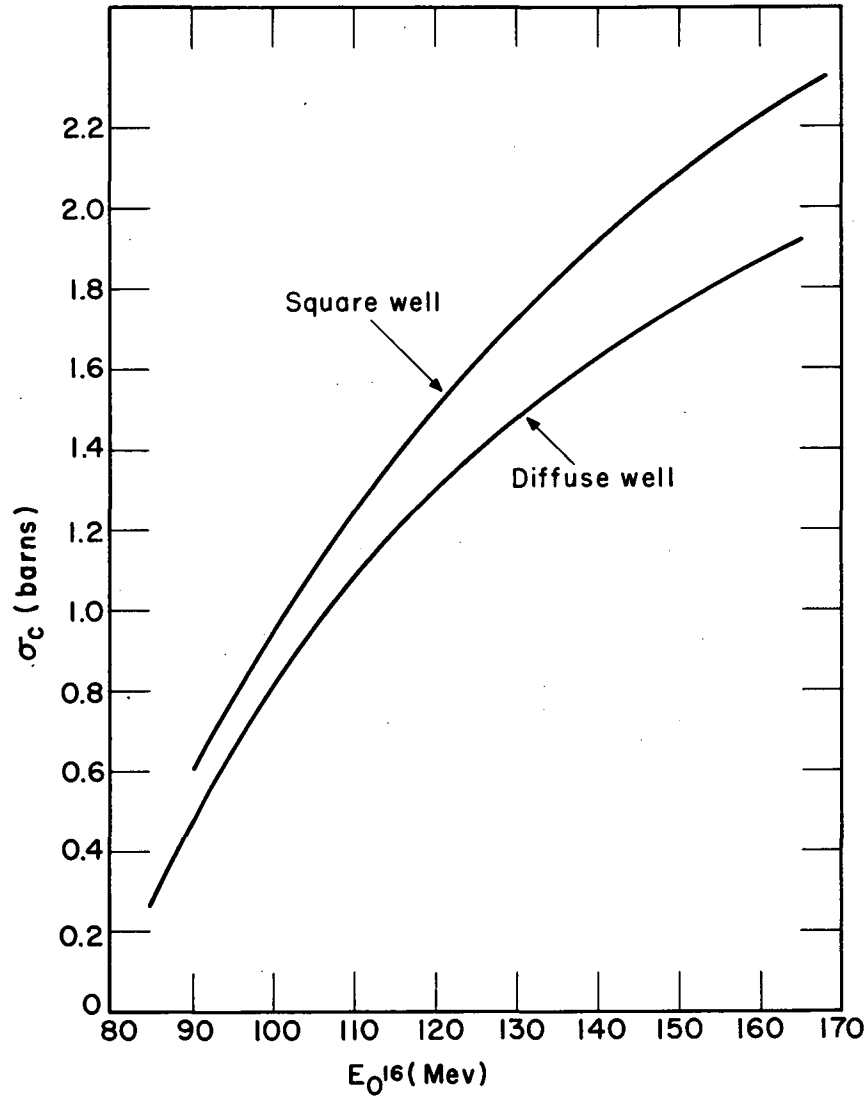
MU-21029

Fig. 23. Cross sections for compound-nucleus formation in the bombardment of Tm^{169} with O^{16} ions.



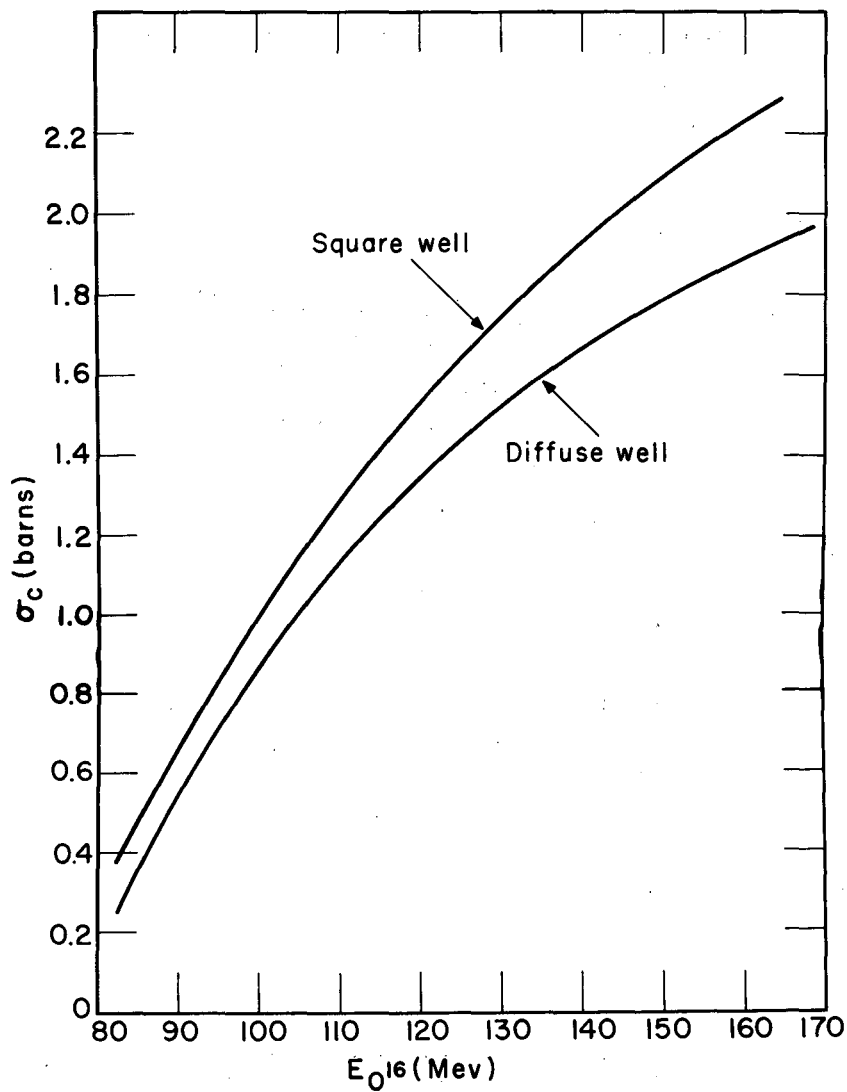
MU-21030

Fig. 24. Cross sections for compound-nucleus formation in the bombardment of Re^{186} with C^{12} ions.



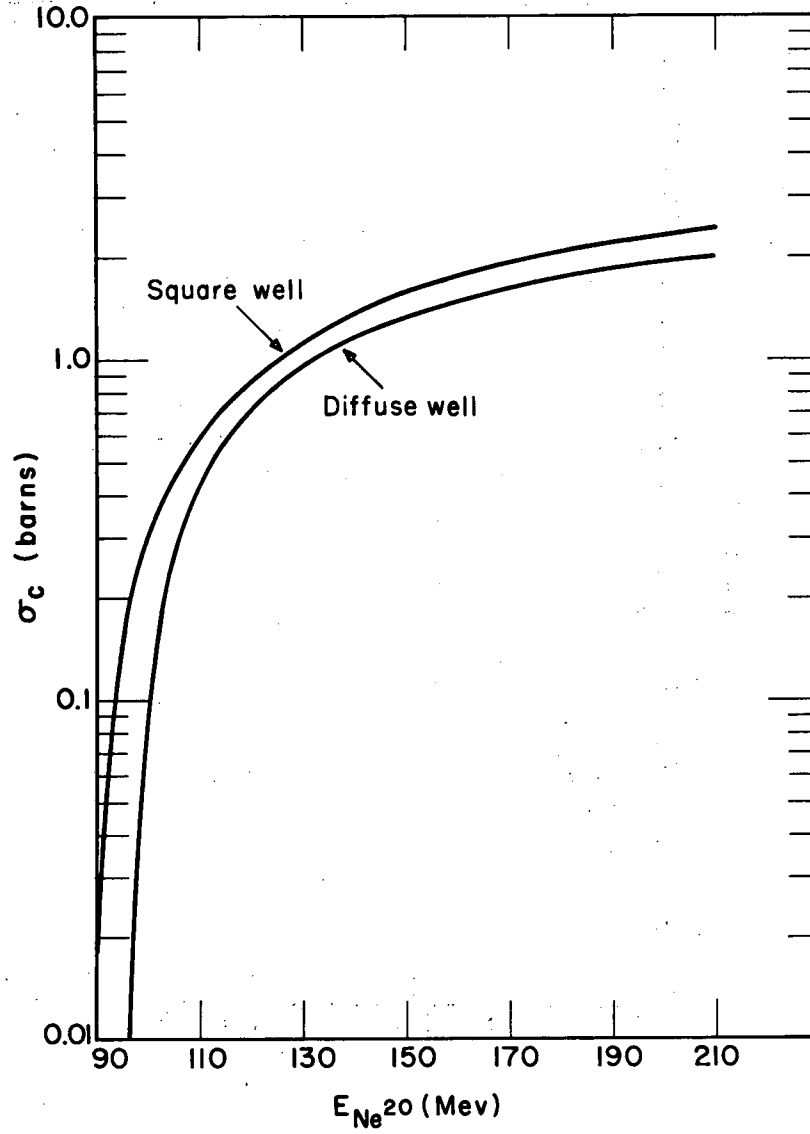
MU-21031

Fig. 25. Cross sections for compound-nucleus formation in the bombardment of Re^{186} with O^{16} ions.



MU-21032

Fig. 26. Cross sections for compound-nucleus formation in the bombardment of Ta^{181} with O^{16} ions.



MU-21033

Fig. 27. Cross sections for compound-nucleus formation in the bombardment of Ta^{181} with Ne^{20} ions.

the equation

$$\ell_{\max} = \left[2\mu(R_1 + R_2)^2 (E_{\text{c.m.}} - B) \right]^{1/2} / \hbar \quad (\text{IV - 1})$$

where

μ = reduced mass of system

$$R_i = 1.5 \times 10^{-13} A_i^{1/3}$$

$E_{\text{c.m.}}$ = center-of-mass energy of system

B = Coulomb barrier

Equation (IV - 1) may be obtained from the sum of Coulomb and maximum centrifugal barriers:

$$E_{\text{c.m.}} = \frac{Z_1 Z_2 e^2}{R_1 + R_2} + \frac{\ell(\ell + 1)}{2\mu(R_1 + R_2)^2} \quad (\text{IV - 2})$$

In Equation (IV - 1) the approximation has been made that for the large values of ℓ encountered in these bombardments, $\ell(\ell + 1) \approx \ell^2$.

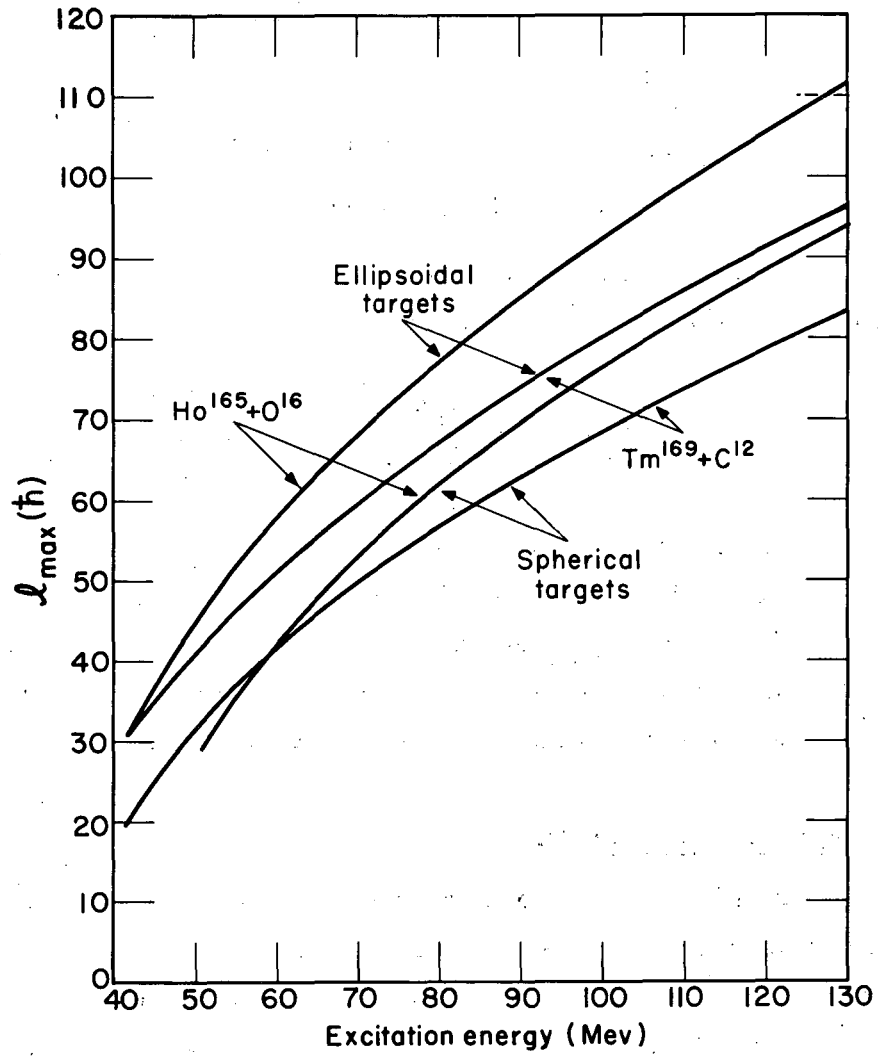
Values of ℓ_{\max} obtained in this way are plotted as a function of excitation energy for pairs of bombarding particles and targets giving the same compound nucleus. (Figs. 28 through 31).

2. Square-Well Model.

In addition to providing compound-nucleus cross sections, the calculations of Thomas have given values of average orbital angular momentum ($\bar{\ell}$). Thomas has shown, however, that results of angular momentum calculations based on the square-well model agree closely with the classical calculation except in the region below the Coulomb barrier. Accordingly, the calculations of the preceding section will be assumed to represent the maximum angular momentum to be associated with the compound-nucleus cross sections obtained in Section IV. A. 1.

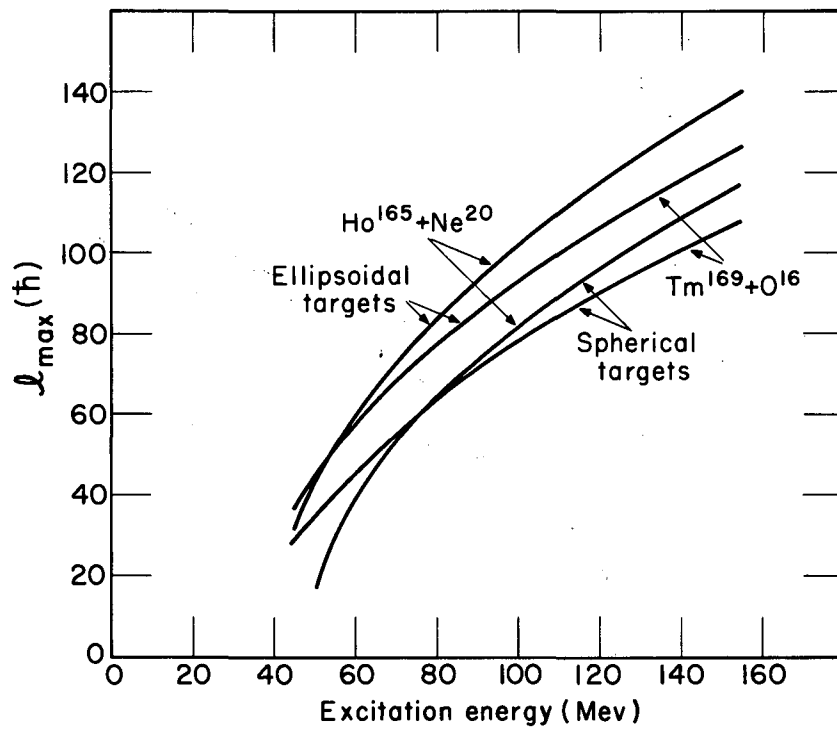
3. Diffuse-Well Model.

The IBM 650 program used for calculation of compound-nucleus cross sections (Section IV. A. 2.) also results in a calculation of the average orbital angular momentum of the system. This average value



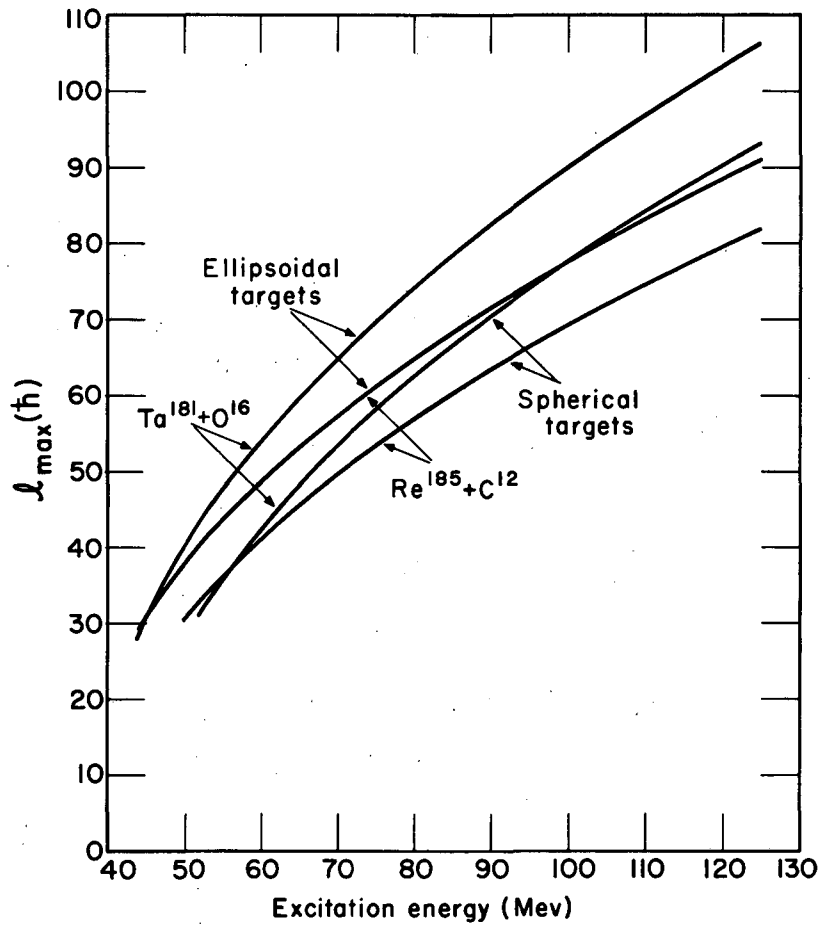
MU-21034

Fig. 28. Maximum angular momentum (classical) as a function of excitation energy in the compound nucleus for $\text{Ho}^{165} + \text{O}^{16}$ and $\text{Tm}^{169} + \text{C}^{12}$.



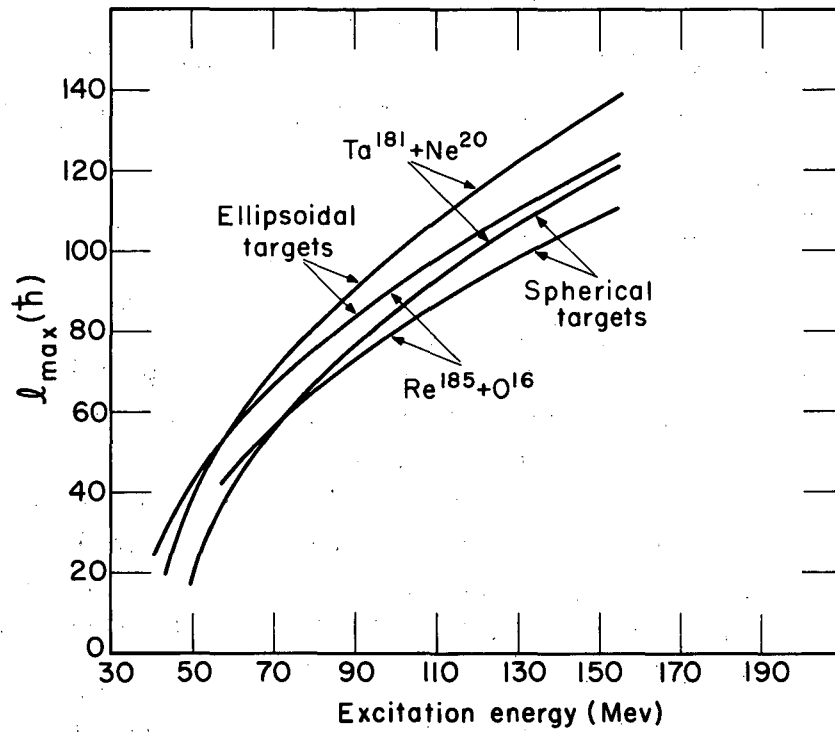
MU-21035

Fig. 29. Maximum angular momentum (classical) as a function of excitation energy in the compound nucleus for $\text{Ho}^{165} + \text{Ne}^{20}$ and $\text{Tm}^{169} + \text{O}^{16}$.



MU-21036

Fig. 30. Maximum angular momentum (classical) as a function of excitation energy in the compound nucleus for Ta¹⁸¹ + O¹⁶ and Re¹⁸⁵ + C¹².



MU-21037

Fig. 31. Maximum angular momentum (classical) as a function of excitation energy in the compound nucleus for $\text{Ta}^{181} + \text{Ne}^{20}$ and $\text{Re}^{185} + \text{O}^{16}$.

is defined as

$$\bar{l} = \frac{\sum l \sigma_l}{\sum \sigma_l} \quad (\text{IV - 3})$$

where $\sigma_l = \pi \lambda^2 (2l + 1) T_l$

T_l = transmission coefficient for the l th wave.

Values of \bar{l} are plotted (Figs. 32 through 35) as a function of excitation energy for pairs of systems giving the same compound nucleus.

C. Excitation Energy.

Excitation energy was calculated from the definition

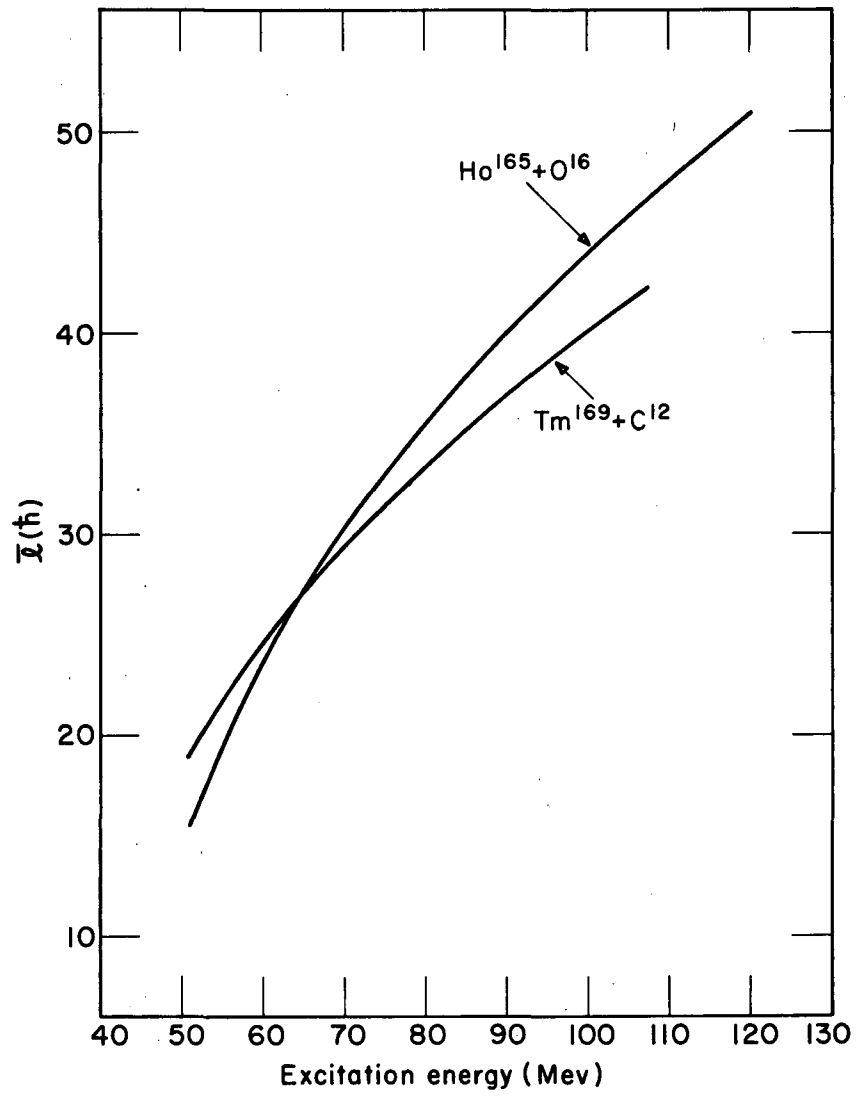
$$E^* = \frac{m_2}{m_1 + m_2} E_1 + (m_3 - m_1 - m_2) c^2 \quad (\text{IV - 4})$$

where E^* = excitation energy of compound nucleus
 m_1 = mass of bombarding particle
 m_2 = mass of target nucleus
 m_3 = mass of compound nucleus (ground state)
 E_1 = bombarding particle energy (lab).

All masses were taken from the tabulation of Gameron.²⁸

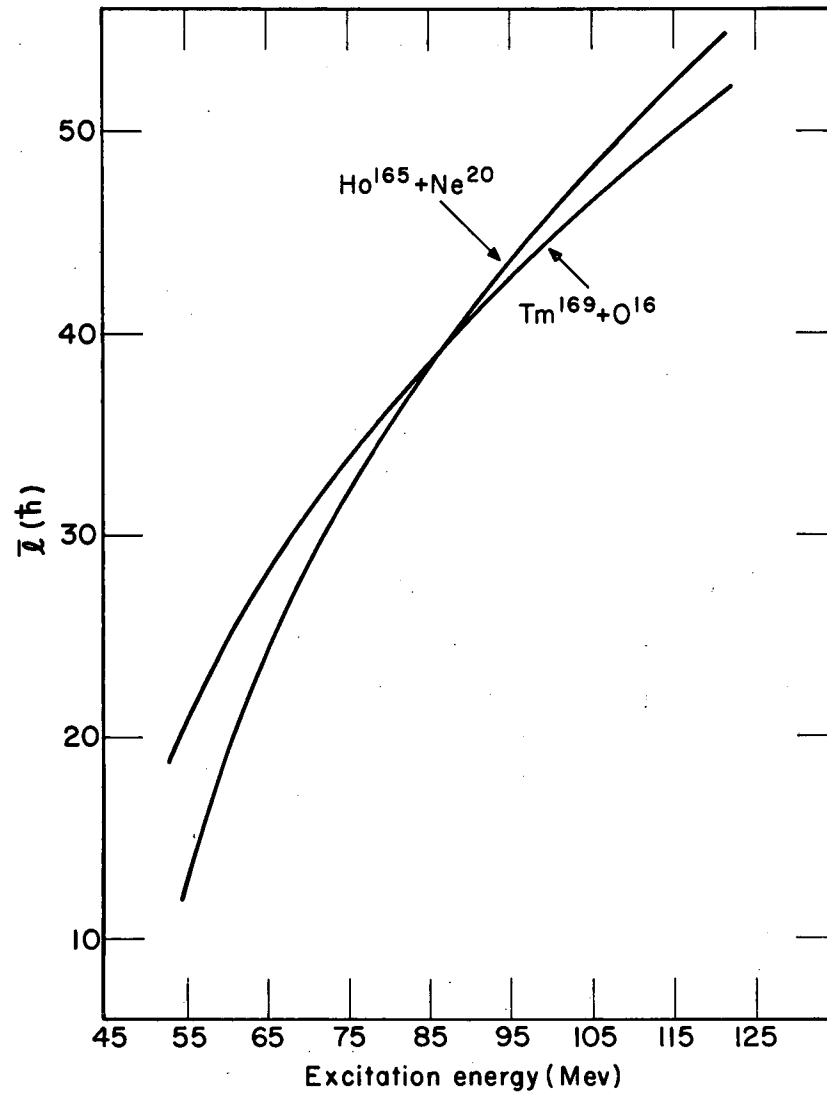
Expressions for E^* obtained by substitution of appropriate masses into (IV - 4) were as follows:

<u>System</u>	<u>E*</u> <u>(Mev)</u>
Ho ¹⁶⁵ + O ¹⁶	0.911 E _O - 21.9
Ho ¹⁶⁵ + Ne ²⁰	0.892 E _{Ne} - 30.2
Tm ¹⁶⁹ + C ¹²	0.935 E _C - 14.2
Tm ¹⁶⁹ + O ¹⁶	0.914 E _O - 25.0
Ta ¹⁸¹ + O ¹⁶	0.919 E _O - 25.6
Ta ¹⁸¹ + Ne ²⁰	0.900 E _{Ne} - 36.3
Re ¹⁸⁵ + C ¹²	0.939 E _C - 16.0
Re ¹⁸⁵ + O ¹⁶	0.920 E _O - 29.3
Re ¹⁸⁷ + C ¹²	0.940 E _C - 14.9



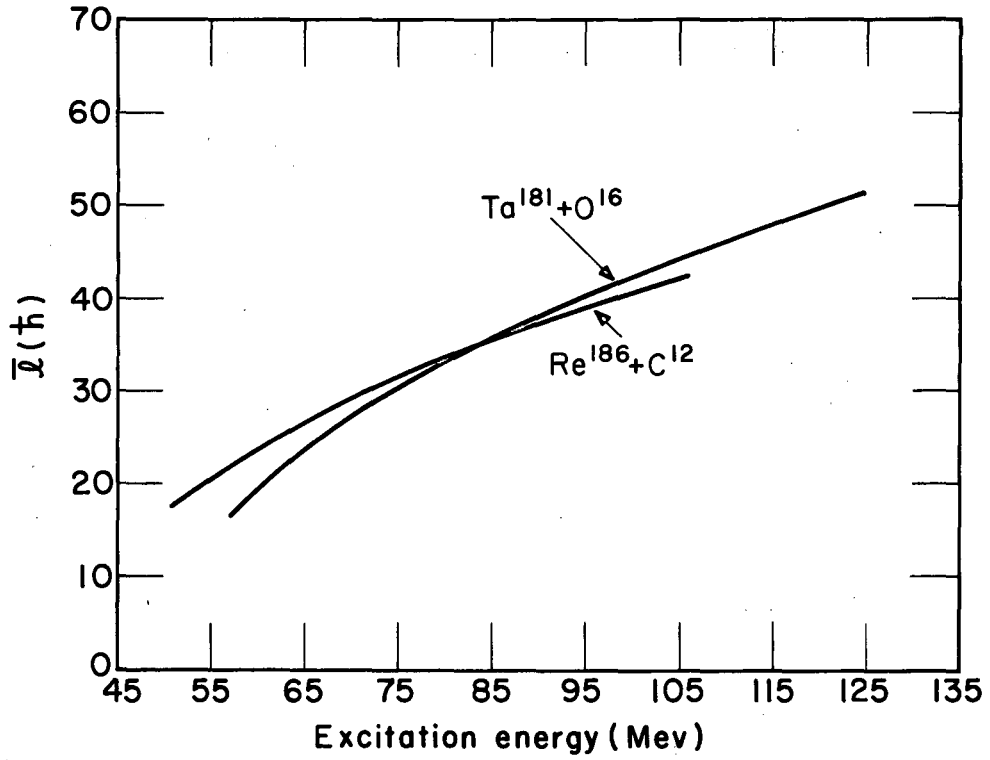
MU-21038

Fig. 32. Average angular momentum as a function of excitation energy in the compound nucleus for $\text{Ho}^{165} + \text{O}^{16}$ and $\text{Tm}^{169} + \text{C}^{12}$ (diffuse-well model).



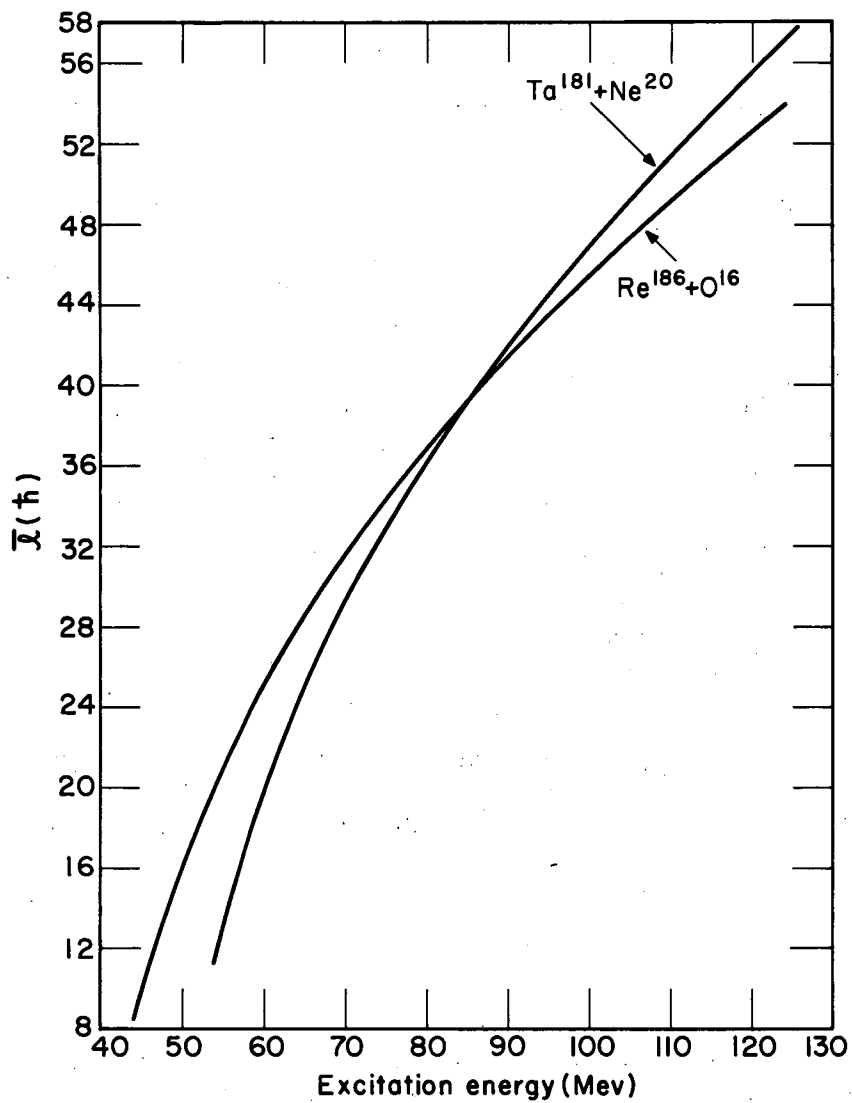
MU-21039

Fig. 33. Average angular momentum as a function of excitation energy in the compound nucleus for $\text{Ho}^{165} + \text{Ne}^{20}$ and $\text{Tm}^{169} + \text{O}^{16}$ (diffuse-well model).



MU-21040

Fig. 34. Average angular momentum as a function of excitation energy in the compound nucleus for $Ta^{181} + O^{16}$ and $Re^{186} + C^{12}$ (diffuse-well model).



MU-21041

Fig. 35. Average angular momentum as a function of excitation energy in the compound nucleus for $Ta^{181} + Ne^{20}$ and $Re^{186} + O^{16}$ (diffuse-well model).

V. RESULTS AND DISCUSSION

A. Fission Probability as a Function of Excitation Energy.

The variation of fission probability, σ_f/σ_c , with excitation energy, E^* , for pairs of targets and bombarding particles giving the same compound nucleus is shown in the following figures.

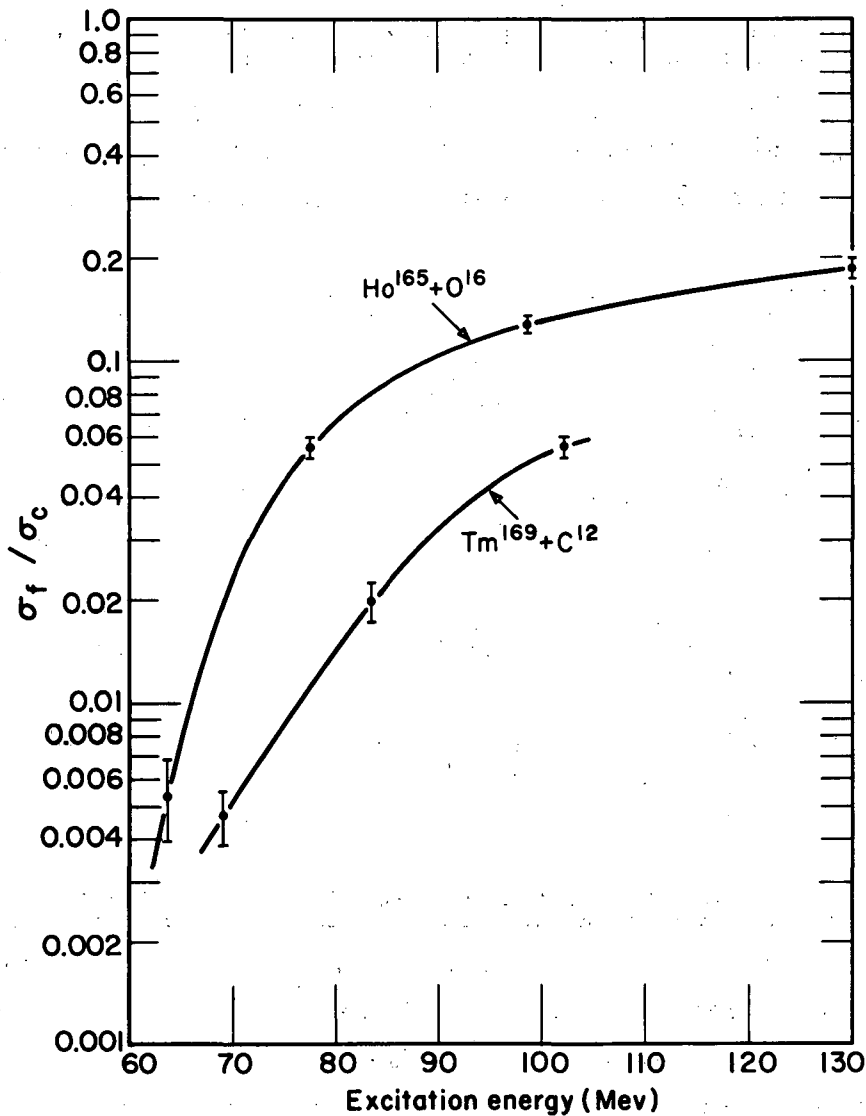
<u>System</u>	<u>Compound nucleus</u>	<u>Square-well σ_c</u>	<u>Diffuse-well σ_c</u>
$\text{Tm}^{169} + \text{C}^{12}$	Re^{181}	Fig. 36	Fig. 40
$\text{Ho}^{165} + \text{O}^{16}$			
$\text{Tm}^{169} + \text{O}^{16}$	Ir^{185}	Fig. 37	Fig. 41
$\text{Ho}^{165} + \text{Ne}^{20}$			
$\text{Re}^{185} + \text{C}^{12}$	Tl^{197}	Fig. 38	Fig. 42
$\text{Ta}^{181} + \text{O}^{16}$			
$\text{Re}^{185} + \text{O}^{16}$	Bi^{201}	Fig. 39	Fig. 43
$\text{Ta}^{181} + \text{Ne}^{20}$			

B. Correlation of Fission Probability and Angular Momentum.

A comparison of values of σ_f/σ_c (Figs. 36 through 43) with corresponding angular momentum values (Figs. 28 through 35) indicates that for a given excitation, a higher fission probability for the heavier ion bombardment in general corresponds to a higher angular momentum brought in by that ion. This correlation is independent of whether the square-well or diffuse-well value of σ_c is used in σ_f/σ_c . Factors governing the relation between σ_f/σ_c and l are discussed in the following sections.

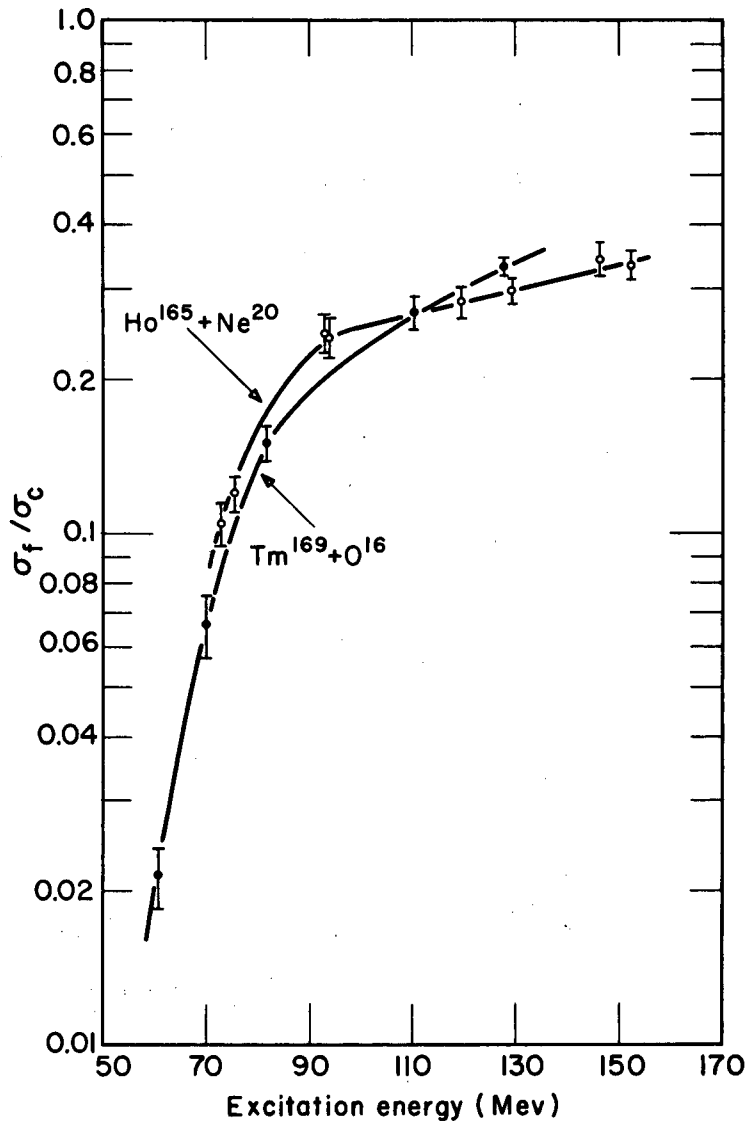
1. Fission Barrier.

A direct effect of angular momentum in increasing σ_f/σ_c is the decrease in the fission barrier suggested by the liquid-drop model



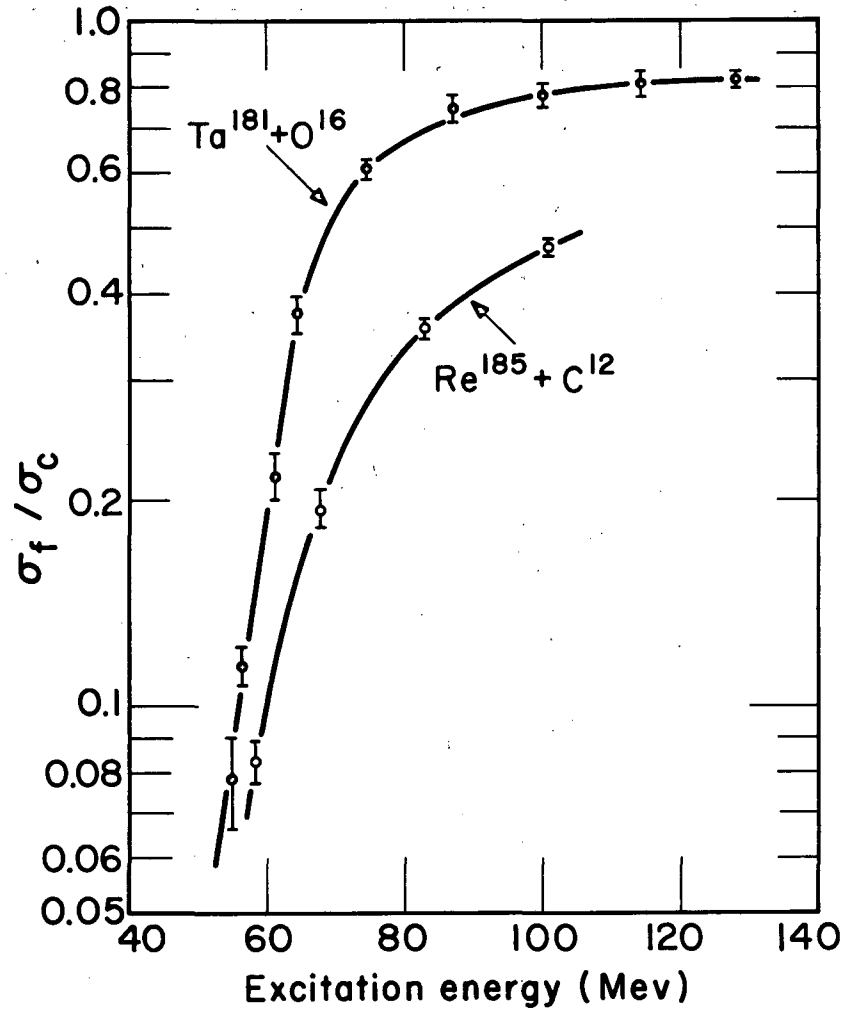
MU-21042 -/

Fig. 36. Probability for fission in the bombardments $\text{Ho}^{165} + \text{O}^{16}$ and $\text{Tm}^{169} + \text{C}^{12}$ (square-well σ_c).



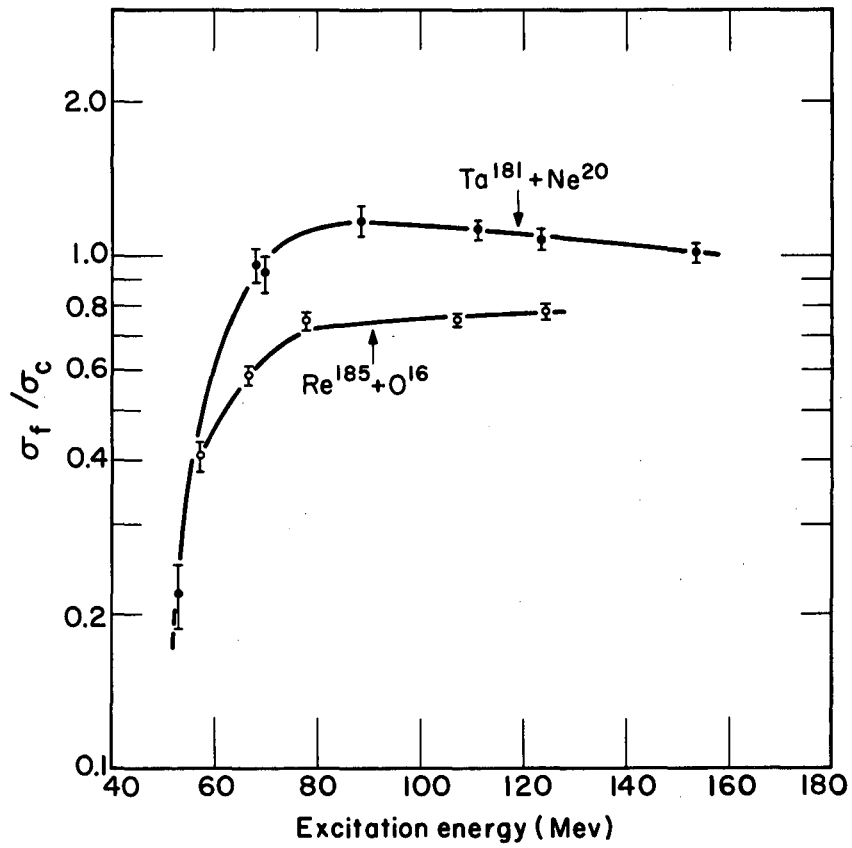
MU-21043 3-7

Fig. 37. Probability for fission in the bombardments $\text{Ho}^{165} + \text{Ne}^{20}$ and $\text{Tm}^{169} + \text{O}^{16}$ (square-well σ_c).



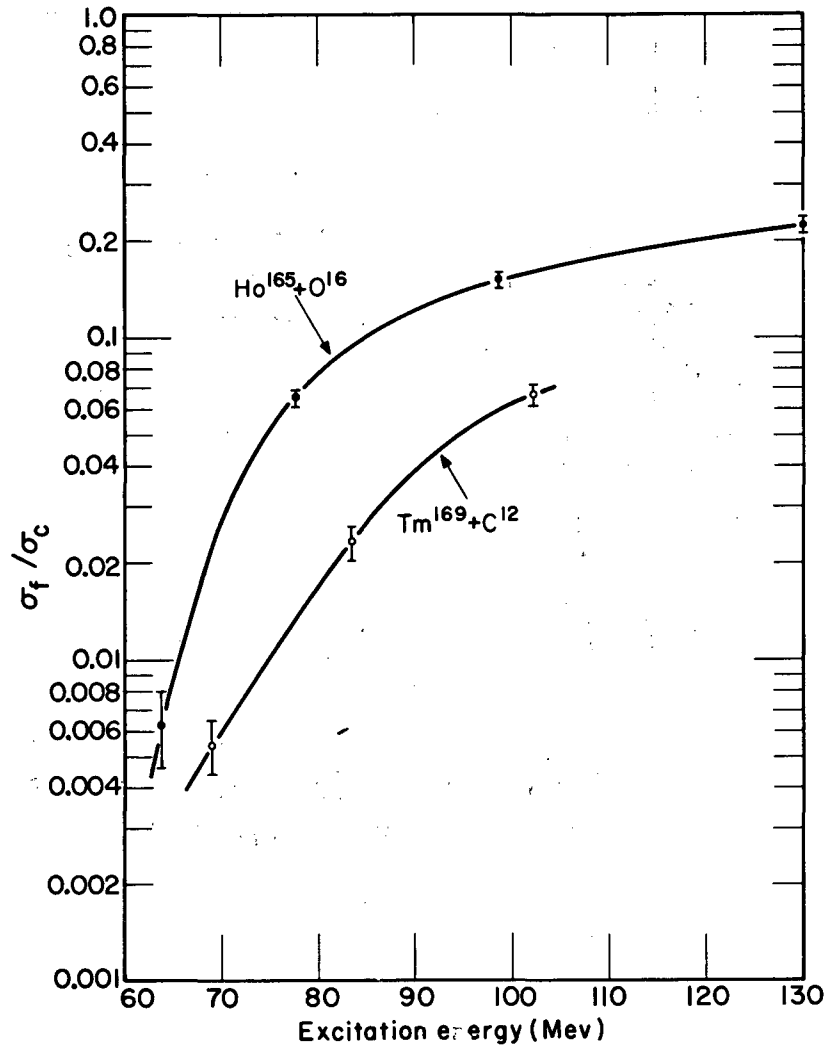
MU - 21044

Fig. 38. Probability for fission in the bombardments $Ta^{181} + O^{16}$ and $Re^{185} + C^{12}$ (square-well σ_c).



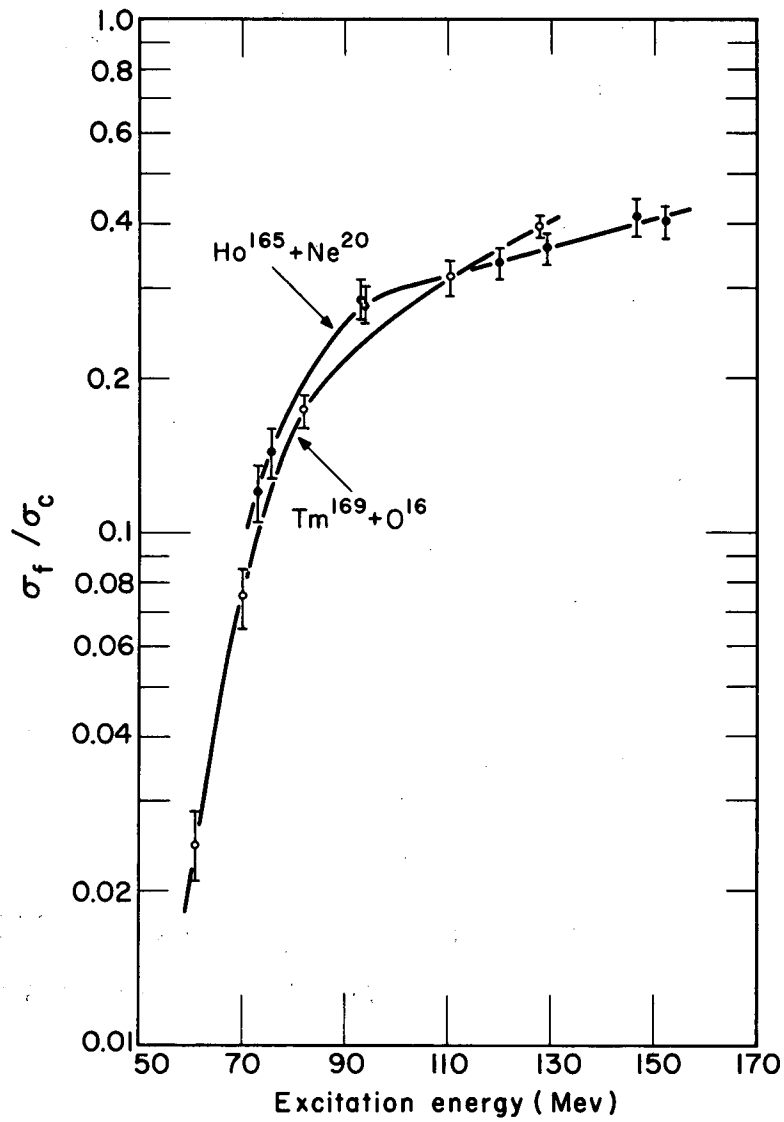
MU-21045

Fig. 39. Probability for fission in the bombardments $Ta^{181} + Ne^{20}$ and $Re^{185} + O^{16}$ (square-well σ_c).



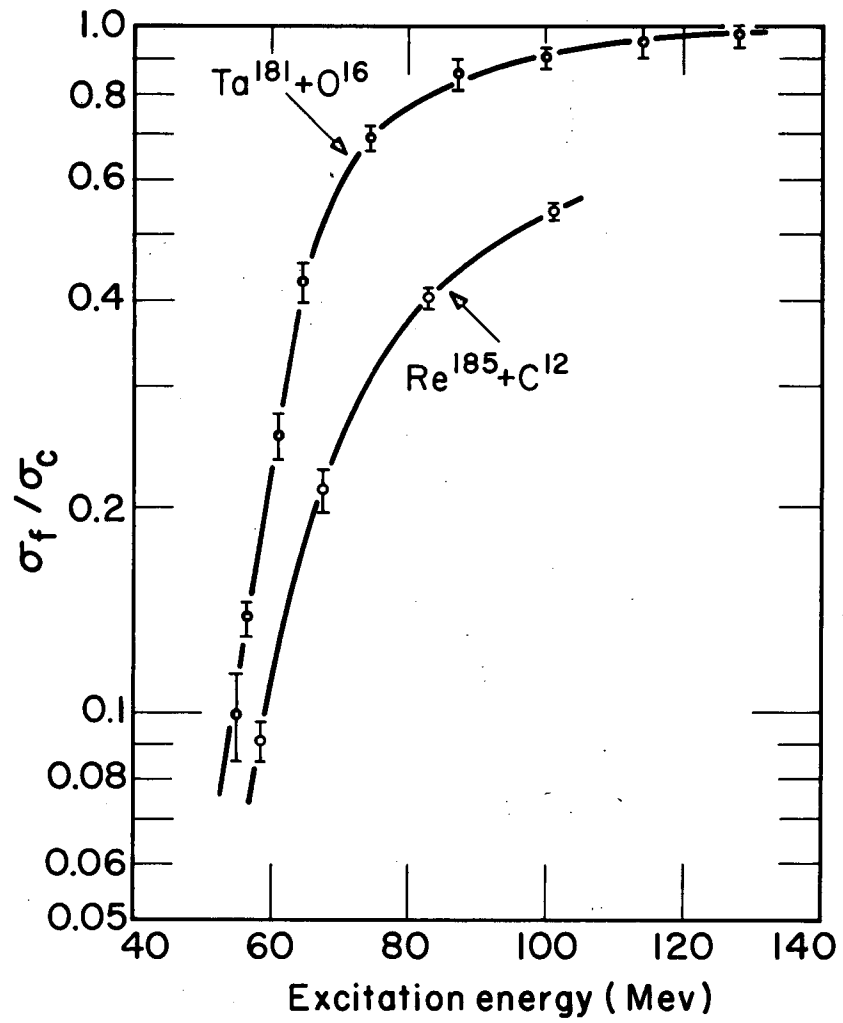
MU-21046

Fig. 40. Probability for fission in the bombardments $\text{Ho}^{165} + \text{O}^{16}$ and $\text{Tm}^{169} + \text{C}^{12}$ (diffuse-well σ_c).



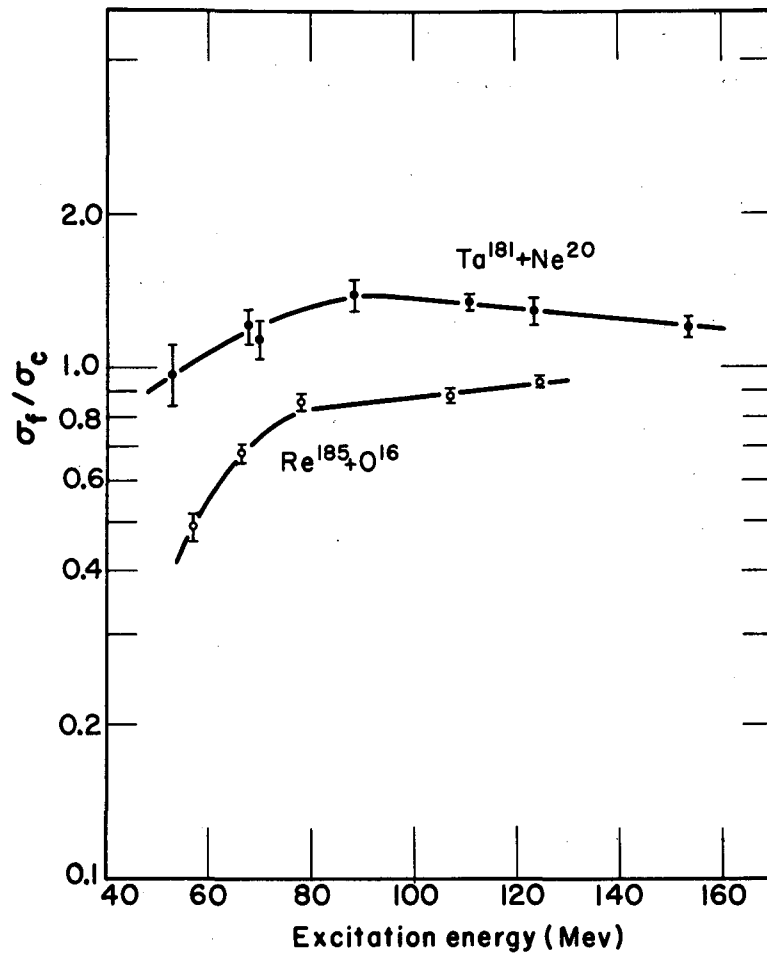
MU-21047

Fig. 41. Probability for fission in the bombardments $\text{Ho}^{165} + \text{Ne}^{20}$ and $\text{Tm}^{169} + \text{O}^{16}$ (diffuse-well σ_c).



MU - 21048

Fig. 42. Probability for fission in the bombardments $Ta^{181} + O^{16}$ and $Re^{185} + C^{12}$ (diffuse-well τ_c).



MU-21049

Fig. 43. Probability for fission in the bombardments $Ta^{181} + Ne^{20}$ and $Re^{185} + O^{16}$ (diffuse-well σ_c).

calculations of Pik-Pichak⁶ and Hiskes.⁷ It should be recognized that these liquid-drop model calculations must be used with caution in interpreting results involving compound nuclei as low in Z^2/A as those studied in this work. It is nevertheless interesting to find the direction and magnitude of angular momentum effects predicted by the model. In Fig. 44 the equation of Hiskes (I - 3) has been used to evaluate the fission barrier, B_f , as a function of angular momentum for Tl^{197} . This is the compound nucleus formed by bombarding Ta^{181} with O^{16} ions or Re^{185} with C^{12} ions. Reference to Fig. 38 shows that for an excitation energy of 101 Mev the value of σ_f/σ_c for $Ta + O$ is 0.78, while σ_f/σ_c for $Re + C$ is only 0.47. From Fig. 30, the maximum angular momentum at $E^* = 101$ Mev is $78 \hbar$ for $Ta + O$ and $70 \hbar$ for $Re + C$. Figure 44 then shows that B_f is decreased from 15.4 Mev to 8.2 Mev because of angular momentum in the $Ta + O$ bombardment and from 15.4 Mev to 9.4 Mev in the $Re + C$ bombardment. The effect of angular momentum on the level width for fission, Γ_f , may be estimated from the expression of Fujimoto and Yamaguchi,²⁹

$$\Gamma_f = \frac{T}{2\pi} \exp(-B_f/T) \quad (V - 1)$$

where

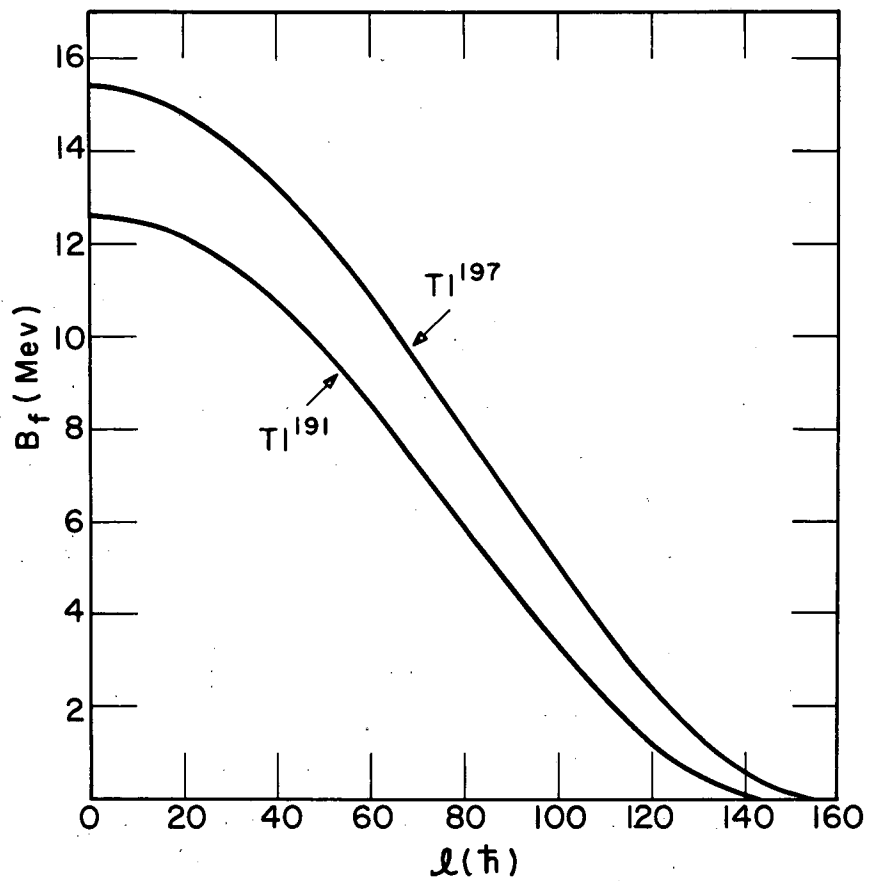
$$T = \left(\frac{10E^*}{A} \right)^{1/2}$$

The derivation of the foregoing expression is based on the assumption that the Fermi gas model is applicable in describing the fissioning nucleus. If one defines the nuclear temperature in the case of fission as referring to excitation at the saddle point, then the energies of deformation and rotation at the saddle point should be subtracted from E^* in the equation for T . This correction is

$$\Delta_{\text{saddle}} = (E_{\text{Coulomb}} + E_{\text{surface}} + E_{\text{rotation}})_{\text{saddle}} - (E_{\text{Coulomb}} + E_{\text{surface}})_{\text{sphere}} \quad (V - 2)$$

From Hiskes's expression⁷ for the saddle point energy,

$$\frac{(E_C + E_s + E_r)_{\text{saddle}}}{(E_s)_{\text{sphere}}} = 1 + 2x + y + \frac{98}{135} z^3 - \frac{7}{6} zy \quad (V - 3)$$



MU-21050

Fig. 44. The barrier for fission of Tl^{191} and Tl^{197} as a function of angular momentum.

where

$$y = \left(\frac{E_f}{E_s} \right)_{\text{sphere}},$$

$$z = 1 - x,$$

and the definition of x,

$$x = \frac{Z^2/A}{(Z^2/A)_{\text{crit.}}} = \left(\frac{E_C}{2E_s} \right)_{\text{sphere}}, \quad (\text{V} - 4)$$

it follows that

$$\frac{\Delta_{\text{saddle}}}{(E_s)_{\text{sphere}}} = y + \frac{98}{135} z^3 - \frac{7}{6} zy. \quad (\text{V} - 5)$$

For the bombardment Ta + O, where $\ell_{\text{max}} = 78\hbar$, Δ_{saddle} is calculated to be 28.5 Mev and $T = 1.92$ Mev. For Re + C ($\ell_{\text{max}} = 70\hbar$), $\Delta_{\text{saddle}} = 25.5$ Mev and $T = 1.96$ Mev.

The ratio of fission level widths for the different angular momenta is

$$\frac{(\Gamma_f)_{\text{Ta} + \text{O}}}{(\Gamma_f)_{\text{Re} + \text{C}}} = \frac{[T \exp(-B_f/T)]_{\text{Ta} + \text{O}}}{[T \exp(-B_f/T)]_{\text{Re} + \text{C}}} = 1.7 \quad (\text{V} - 6)$$

It must be emphasized that this 70% increase in Γ_f refers only to fission of the initial compound nucleus Tl^{197} , formed with the maximum angular momentum. Analyses of fission and $(\text{N}^{14}, \text{xn})$ cross sections for N^{14} bombardment of Au^{197} have shown that fission occurs principally in nuclei resulting from emission of several neutrons from the compound nucleus.²² This result may be interpreted in terms of two effects. An increase in neutron binding energies coupled with a decreasing fission barrier as neutrons are evaporated gives an increased probability for fission relative to neutron emission. In terms of the liquid-drop model the lowering of B_f with neutron emission is related to an increase in Z^2/A , which is proportional to the ratio of disruptive Coulomb energy to stabilizing surface energy. The effect of the loss of six neutrons on B_f may be seen in Fig. 44, where plots of B_f for Tl^{197} and Tl^{191} are shown. A reduction in B_f due to angular momentum would be expected to accompany the reduction in B_f due to neutron emission

since the neutron can remove only a small fraction of the initial angular momentum of the compound nucleus.

2. Neutron and Charged-Particle Emission.

The effect of angular momentum on the competing de-excitation modes of neutron and charged-particle emission is also reflected in fission probability. Halpern has suggested that the rotational energy of a nucleus is unavailable for neutron evaporation and should be added to the neutron binding energy in the determination of the level width for neutron emission.⁴ If neutron emission may be considered to occur from a nucleus that has reached equilibrium with respect to changes in surface, Coulomb, and rotational energies, the excitation energy that has become available for neutron emission is:

$$\Delta_{eq} = (E_s + E_C + E_r)_{eq} - (E_C + E_s)_{sphere} \quad (V-7)$$

This term may be evaluated from Hiskes's expression for the deformation and rotation energy of the equilibrium configuration of the rotating liquid drop⁷

$$\frac{(E_s + E_C + E_r)_{eq}}{(E_s)_{sphere}} = 1 + 2x + y + \frac{7}{6}zy + \frac{49}{135}z^3 - \left(\frac{2}{3}y + \frac{14}{45}z^2\right)\left(\frac{49}{36}z^2 + \frac{35}{12}y\right)^{1/2} \quad (V-8)$$

$$\frac{\Delta_{eq}}{(E_s)_{sphere}} = y + \frac{7}{6}zy + \frac{49}{135}z^3 - \left(\frac{2}{3}y + \frac{14}{45}z^2\right)\left(\frac{49}{36}z^2 + \frac{35}{12}y\right)^{1/2} \quad (V-9)$$

Considering again the formation of Tl^{197} at $E^* = 101$ Mev and l_{max} , values of Δ_{eq} are calculated to be 19.6 Mev for the Ta + O bombardment ($l_{max} = 78\hbar$) and 16.0 Mev for the Re + C bombardment ($l_{max} = 70\hbar$). The difference in level widths for neutron emission in the two bombardments may then be estimated from the expression of Fujimoto and Yamiguchi:²⁹

$$\Gamma_n = \frac{A^{2/3} T^2}{\pi K} \exp(-B_n/T) \quad (V-10)$$

where $K = \hbar^2 / 2(\text{mass})_n r_0^2$.

Instead of adding Δ_{eq} to B_n , it appears more reasonable to regard it as unavailable as excitation for evaporation of the neutron. The quantity Δ_{eq} is accordingly subtracted from E^* in the expression for T in (V - 1).

Then:

$$\frac{(\Gamma_n)_{Ta + O}}{(\Gamma_n)_{Re + C}} = \frac{\exp(-B_n/T)_{Ta + O}}{\exp(-B_n/T)_{Re + C}} = 0.88 \quad (V - 11)$$

A value of 8.15 Mev²⁸ for B_n was used in the above calculation.

The level width for charged-particle emission should suffer a similar reduction, due to the unavailability of rotational and distortion energies. In this case, however, the level width expression²⁹ contains a potential barrier term, V . For alpha particle emission,

$$\Gamma_\alpha = \frac{A^{2/3} T^2}{\pi K} \exp - [(B_\alpha + V_\alpha)/T]. \quad (V - 12)$$

Knox, Quinton, and Anderson have pointed out that the barrier against charged-particle emission is reduced in the region of sharpest curvature of the deformed rotating nucleus.³⁰ The magnitude of the reduction in V may be estimated from the work of Hiskes.⁷ His expression for the potential at the surface of the drop is, to first order in the deformation parameter a_{20} ,

$$\frac{V_{\text{deformed}}}{V_{\text{sphere}}} = 1 - \frac{1}{5} a_{20} (3 \cos^2 \theta - 1) \quad (V - 13)$$

where θ is the angle between the radius vector and the axis of rotation.

The deformation parameter, a_{20} , is the fractional change in length of the axis of rotation.

$$a_{20} = \frac{7}{6} z + \frac{5}{3} y - \left[\left(\frac{7}{6} z + \frac{5}{3} y \right)^2 + \frac{35}{12} y \right]^{1/2}. \quad (V - 14)$$

For the Ta + O bombardment ($\ell_{\text{max}} = 78\hbar$), a_{20} is found to be -0.115 indicating that the equilibrium configuration is an oblate spheroid

with coincident axes of symmetry and rotation. From Expression (V - 13) the change in surface potential at the equator of the drop is

$$\frac{V_{\text{deformed}}}{V_{\text{sphere}}} = 1 - \frac{1}{5}(-0.115)(3 \cos^2 \frac{\pi}{2} - 1) = 0.976 \quad (\text{V} - 15)$$

The potential barrier for alpha emission from Tl^{197} is thus reduced from 21.0 Mev to $(0.976)(21.0) = 20.5$ Mev. For the $\text{Re} + \text{C}$ bombardment ($\ell_{\text{max}} = 70\hbar$) the corresponding reduction is from 21.0 Mev to 20.6 Mev.

The ratio of alpha-emission level widths for these two cases is then

$$\frac{(\Gamma_{\alpha})_{\text{Ta} + \text{O}}}{(\Gamma_{\alpha})_{\text{Re} + \text{C}}} = \frac{\left\{ T^2 \exp \left[- (B_{\alpha} + V_{\alpha})/T \right] \right\}_{\text{Ta} + \text{O}}}{\left\{ T^2 \exp \left[- (B_{\alpha} + V_{\alpha})/T \right] \right\}_{\text{Re} + \text{C}}} = 0.84. \quad (\text{V} - 16)$$

It may be seen that that small reductions in V_{α} are not sufficient to compensate for the decrease in T due to subtraction of deformation and surface energy.

Despite the indicated suppression of charged-particle emission, the following considerations suggest that evaporation of charged particles occurs with significant probability at the relatively high excitation energies involved in these experiments.

In the bombardment of Re^{187} with C^{12} ions to give Tl^{199} nuclei excited to 102 Mev, the quantity σ_f/σ_c was found to be 0.38. Consider a number N of Tl^{199} nuclei to be formed in the $\text{Re}^{187} + \text{C}^{12}$ bombardment. A number N' of these lose two neutrons and an average energy of 10 Mev per neutron ($B_n + 2T$) in reaching the stage Tl^{197} excited to approx 82 Mev. From Fig. 38, bombardment of Ta^{181} with O^{16} , giving Tl^{197} excited to 82 Mev results in a value for σ_f/σ_c of 0.68. If 0.68 is also considered to be the fraction of N' Tl^{197} nuclei undergoing fission, then the total number of fissions from the Re^{187} bombardment is $0.68 N' + X$, where X is the number of fissions of nuclei that have not passed through the stage Tl^{197} . The ratio of total fissions to compound nuclei formed is

$$\frac{0.68 N' + X}{N} = \frac{\sigma_f}{\sigma_c} = 0.38. \quad (\text{V} - 17)$$

If in one limit it is assumed that no Tl^{199} nuclei emit two neutrons to reach the stage Tl^{197} , then $X/N = 0.38$. Fission occurs then only in nuclei that have not passed through the Tl^{197} stage and $(1-0.38)N$ nuclei neither fission nor pass through Tl^{197} .

Assume in the other limit that all fissions are of nuclei that have passed through Tl^{197} , i. e., $X = 0$. As a result, $0.68 N'/N = 0.38$; $N'/N = 0.56$, and a number $(1-0.56)N$ Tl^{199} nuclei neither fission nor pass through Tl^{197} . It appears then that between 0.44 and 0.62 of the initial compound nuclei emit a charged particle or particles at an early stage of the de-excitation process. Prompt emission of an alpha particle would remove an average excitation of the order of the alpha barrier energy, in addition to a few units of angular momentum and two units of atomic number. The latter factors would be reflected in an increased fission barrier and might be critical in determining whether the nucleus could fission at a later stage.

Inclusion of angular momentum in the foregoing comparisons does not change the result significantly. For Tl^{199} l_{max} is calculated as $70\hbar$. For Tl^{197} from $Ta^{181} + O^{16}$ ($E^* = 82$) l_{max} is $64\hbar$. Since Tl^{197} formed by loss of two neutrons from Tl^{199} should have l_{max} of at least $64\hbar$, it seems appropriate to use 0.68 as the lower limit for the fraction of N' nuclei which fission. A number larger than 0.68 would increase the lower limit of nuclei which neither fission nor pass through Tl^{197} .

Evidence has also been presented for a high probability of alpha-particle emission in the bombardment of Au^{197} with 160-Mev O^{16} ions. In an experiment in which alpha-particle energy spectra and angular distributions were measured, Knox et al.³⁰ determined a value of 1.0 ± 0.3 barns for the cross section for alpha-particle production. A strong forward peaking of the angular distribution suggests, however, that some of the alpha particles arise through a direct interaction mechanism.

Still other evidence for pre-fission alpha emission has been obtained by Blann in a study of the charge distribution of fission fragments in the bombardment of Au^{197} with 112-Mev C^{12} ions.²³ And for this same system, Gordon has compared the sum of fission and neutron-evaporation cross sections with the compound-nucleus formation cross section and concluded that charged-particle emission is a significant reaction.³⁹

C. Factors Affecting Compound-Nucleus Formation and Angular Momentum.

Several factors are present in heavy-ion bombardments which introduce uncertainties into the calculation of σ_c and ℓ . Some of these are discussed in the following sections.

1. The σ_c and ℓ Calculations of Thomas.

Blatt and Weisskopf's square-well potential model,²⁷ adapted by Thomas²⁶ to heavy-ion bombardments, has been successful in describing compound-nucleus formation for alpha-particle and lighter-ion bombardments.³¹ Polikanov and Druin³² report that a classical approximation to Blatt and Weisskopf's calculation,

$$\sigma_c = \pi r_0^2 (A_1^{1/3} + A_2^{1/3})^2 (1 - B/E) \quad (V - 18)$$

where $r_0 = 1.4$ to 1.55×10^{-13} cm

B = Coulomb barrier

E = bombarding energy,

agrees closely with measured fission cross sections for bombardment of bismuth and uranium with C^{12} , N^{14} , and O^{16} ions. Recently Sikkeland et al.³³ have measured fission cross sections for the bombardment of U^{238} with C^{12} ions and have found them equal, within experimental error, to Thomas's square-well calculation of σ_c ($r_0 = 1.5 \times 10^{-13}$ cm). In bombarding a target as fissionable as uranium, it cannot be assumed, however, that fission occurs only following formation of a compound nucleus.

Sikkeland et al. have, in fact, found evidence in fission fragment angular distributions that a portion of the fissions are excited by a mechanism other than compound-nucleus formation.³³

The target nuclei used in this work were sufficiently low in Z^2/A so that penetration or "pickup" of only a few nucleons of the bombarding particle would be unlikely to result in fission. For the bombardment of Ta^{181} with Ne^{20} , however, the fission cross section is observed to exceed the calculated compound-nucleus cross sections at moderately

high energies (Figs. 39 and 43). The value of σ_f/σ_c then decreases at still higher energies.

This latter effect cannot be understood in terms of the influence of angular momentum on fission and particle emission level widths, inasmuch as the widths would be expected to change in such ways as to increase fission probability. A similar effect is observed in the bombardment of Ho¹⁶⁵ with Ne²⁰ ions (Figs. 37 and 41). In the vicinity of $E^* = 110$ Mev the quantity σ_f/σ_c for Ho + Ne is observed to fall below the curve of σ_f/σ_c for Tm + O although ℓ_{\max} is larger in the former bombardment. An interesting possibility in explaining these apparent changes of σ_f/σ_c in the regions of very large angular momentum in the Ne²⁰ bombardments is that a critical angular momentum is reached for which the formation of a compound nucleus is forbidden. On the basis of the liquid-drop model, Pik-Pichak⁶ and Hiskes⁷ have determined that for $y > \frac{7}{5}z^2$ an equilibrium configuration of the liquid drop cannot exist. The possibility of some type of interaction between the heavy ion and the target nucleus would not be excluded, but the formation of a compound system in equilibrium with respect to Coulomb, surface, and rotational energies would be forbidden.

The limiting angular momentum corresponding to $\frac{7}{5}z^2$ would be about $150\hbar$ for the bombardments of Ho¹⁶⁵ and Ta¹⁸¹ with Ne²⁰ ions. This value is somewhat larger than the values of ℓ_{\max} calculated for these bombardments (Figs. 29 and 31) but consideration of the approximate nature of the liquid-drop calculations admits the possibility that such an effect may occur.

The square-well compound-nucleus cross sections (with $r_0 = 1.5 \times 10^{-13}$ cm) are seen to exceed the diffuse-well compound-nucleus cross sections at all energies. The relative magnitudes of σ_f/σ_c for each pair of targets and particles are similar for the two σ_c calculations except in the case of Ta + Ne and Re + O. For the lowest energy point in the bombardment of Ta¹⁸¹ with Ne²⁰ the energy of the ion is low enough (99 Mev) to be in the region where the parabolic barrier of the diffuse-well model causes a very rapid decline of σ_c relative to the change for the square-well σ_c .

With the exception of the high energy region of the Ho¹⁶⁵ + Ne²⁰ bombardment the value of σ_f/σ_c for the heavier ion always exceeds

σ_f/σ_c for the lighter ion at a given excitation energy. However, the angular momentum curves for each pair of bombardments are observed to cross in the vicinity of the Coulomb barrier for the square-well calculation and at a somewhat higher energy for the diffuse-well calculation. This crossover is related to the higher Coulomb barrier for the heavier ion (Eq. IV - 1). It appears then that below this point where the angular momentum curves cross, a higher value of σ_f/σ_c is associated with less angular momentum in the compound nucleus. In attempting to explain this result, it would be of interest to examine the distribution of l values brought in by the heavy ion. Although values of σ_c and \bar{l} may be obtained by interpolation into the tabulations of Thomas, it is not possible to obtain the distribution of l values in this manner. At bombarding energies well above the Coulomb barrier, the distribution begins to resemble the distribution for zero barrier, i. e., $\sigma_c \propto 2l + 1$, and a correlation of σ_f/σ_c with l_{\max} should be justified. But at energies at which the distribution becomes barrier-dependent, substantially different distributions may be associated with the same value of l_{\max} in bombardments with two different ions. It is also in the vicinity of the barrier that uncertainties in σ_c and l due to effects such as those discussed in the following section become most important.

2. Deformation of Target Nuclei.

The isotopes used as targets in this work are characterized by strong deformation of the ground state configuration. Professor John O. Rasmussen has suggested that this fact be considered in calculating the maximum angular momentum brought in by a heavy ion. Equation (IV - 1) for the classical value of l_{\max} is modified by the addition of the quadrupole potential and by substitution of the semi-major axis of an ellipsoidal nucleus for the radius of the target.

$$l_{\max} = \left[2\mu(R_1 + R_2)^2 \left(E_{\text{c.m.}} - \frac{Z_1 Z_2 e^2}{R_1 + R_2} - \frac{Z_1 Q_0 e^2}{2(R_1 + R_2)^3} \right) \right]^{1/2} / \hbar \quad (\text{V - 19})$$

where Q_0 = quadrupole moment

R_2 = semi-major axis of target nucleus.

From the work of Bohr³⁴

$$R_2 \approx R_2^{(0)} \left[1 + \sqrt{\frac{5}{4\pi}} \frac{\delta}{0.95} \right] \quad (V-20)$$

where $R_2^{(0)} = 1.5 A_2^{1/3} \times 10^{-13}$ cm.

Values of the deformation parameter, δ , were taken from the work of Mottelson and Nilsson³⁵ and Q_0 values from the tabulation of Alder et al.³⁶ Values of ℓ_{\max} are plotted (Figs. 28 through 31) as a function of excitation energy for pairs of targets and bombarding particles giving the same compound nucleus. It is seen that a substantial increase in ℓ_{\max} has resulted from including the deformed character of the target nuclei in the calculation. A higher value for ℓ_{\max} should also be reflected in an increased compound-nucleus cross section.

3. Polarization Effects.

The relatively large charge of the heavy ion suggests that a mutual polarization of the target and approaching particle may occur with subsequent changes in the Coulomb barrier. Breit, Hull, and Gluckstern³⁷ have used the liquid-drop model to determine the nature of the deformation induced in a U^{238} nucleus as an O^{16} ion approaches. The nucleus was found to flatten along the line of approach and for this case one would expect the Coulomb barrier to increase.

In a liquid-drop model calculation suggested by Dr. W. J. Swiatecki,³⁸ a somewhat different effect was found. Here the target and bombarding particle were restricted to remain in contact, but deformation of both into ellipsoids was permitted. For charged liquid drops corresponding in mass and charge to a Ne^{20} bombarding particle and a Ho^{165} target, a minimum in the sum of deformation and interaction Coulomb energies was found for a configuration in which both nuclei had deformed into prolate ellipsoids with coincident symmetry axes. The ratio of major to minor axes was approximately 1.5 for both nuclei and the Coulomb barrier was about 89% of that for spherical nuclei in contact. An estimate of the probability that the approaching nuclei could depart from the energetically more favorable oblate deformation and reach

this saddle point with lowered Coulomb barrier would require consideration of the amplitude of oscillations between oblate and prolate shapes. In any event one should recognize that changes in Coulomb barrier as a result of polarization may effect substantial differences in values of σ_c and l relative to the calculation for spherical nuclei.

ACKNOWLEDGMENTS

I wish to express my appreciation to Professor Isadore Perlman and to Dr. Stanley G. Thompson for their encouragement and guidance throughout the course of this work.

I am grateful to Dr. Eugene Goldberg and Dr. Harry L. Reynolds for the use of their scattering chamber and for assistance in several phases of this work.

Discussions of the theoretical aspects of this work with Dr. Glen E. Gordon, Dr. John R. Hiskes, Dr. Torbjørn Sikkeland, Dr. Wladyslaw J. Swiatecki, and Mr. Victor E. Viola were greatly appreciated.

I am indebted to Dr. T. Darrah Thomas for making available his computer program and to Professor John O. Rasmussen for assistance with calculations involved in this work.

The cooperation of Mr. Harry Bowman and Mr. Dan O'Connell in obtaining targets was appreciated.

The assistance of Miss Arlene Fregulia and Mr. Maurice de Villers in scanning is gratefully acknowledged.

I wish to acknowledge to my wife, Judy, my indebtedness for help in calculations and for encouragement throughout the course of this work.

This work was performed under the auspices of the United States Atomic Energy Commission.

REFERENCES

1. James F. Miller, Reactions of Fast Carbon Nuclei in Emulsions (Ph. D. thesis), UCRL-1902, July 1952.
2. J. H. Fremlin, *Physica* 22, 1091 (1956).
3. V. A. Druin, S. M. Polikanov, and G. N. Flerov, *Soviet Physics - JETP* 5, 1059 (1957).
4. I. Halpern, *Ann. Rev. Nuclear Sci.* 9, 245 (1959).
5. E. L. Kelly and C. Wiegand, *Phys. Rev.* 73, 1135 (1948).
6. G. A. Pik-Pichak, *Soviet Physics - JETP* 7, 238 (1958).
7. John R. Hiskes, The Liquid-Drop Model of Fission; Equilibrium Configurations and Energetics of Uniform Rotating Charged Drops (Ph. D. thesis) UCRL-9275, June 1960.
8. E. Goldberg and H. L. Reynolds, *Phys. Rev.* 112, 1981 (1958).
9. E. Goldberg, H. L. Reynolds, and D. D. Kerlee, Elastic Scattering of Heavy Ions by Gold and Bismuth, UCRL-5844, Jan. 1960.
10. R. Levi and G. A. Espersen, *Phys. Rev.* 78, 231 (1950).
11. C. C. Dilworth, G. P. S. Occhialini and L. Vermaesen, in Fundamental Mechanisms of Photographic Sensitivity (Symposium) (Butterworth's Scientific Publications, London, 1951), p. 297.
12. G. W. W. Stevens, *ibid.*, p. 310.
13. H. H. Heckman, B. L. Perkins, W. G. Simon, F. M. Smith, and W. H. Barkas, *Phys. Rev.* 117, 544 (1960).
14. J. S. Blair, *Phys. Rev.* 95, 1218 (1954).
15. J. A. McIntyre, S. D. Baker, and T. L. Watts, *Phys. Rev.* 116, 1212 (1959).
16. Edward L. Hubbard, Range-Energy Relation for Heavy Ions in Metals, UCRL-9053, Jan. 1960.
17. Torbjørn Sikkeland (Lawrence Radiation Laboratory), private communication.
18. Glen E. Gordon, Almon E. Larsh, and Torbjørn Sikkeland, Angular Distribution of Fragments from Fission of Au¹⁹⁷ with Carbon Ions, UCRL-9003, Dec. 1959.
19. Victor E. Viola and T. Darrah Thomas (Lawrence Radiation Laboratory), private communication.

20. E. Goldberg and H. L. Reynolds (Lawrence Radiation Laboratory - Livermore) private communication.
21. A. R. Quinton, H. C. Britt, W. J. Knox, and C. E. Anderson, Bull. Am. Phys. Soc. II 4, 414 (1959).
22. N. I. Tarantin, Iu. B. Gerlit, L. I. Guseva, B. F. Miasoedov, K. V. Filippova, and G. N. Flerov, Soviet Physics - JETP 7, 220 (1958).
23. H. Marshall Blann, Fission of Gold with 112-Mev C^{12} Ions: a Yield-Mass and Charge-Distribution Study (Ph. D. thesis), UCRL-9190, May 1960.
24. J. Terrell, as presented by R. B. Leachman, Second United Nations Conference, Geneva, 15, 231 (1958).
25. J. B. Marion, T. I. Arnette, and H. C. Owens, ORNL-2574 (1959).
26. T. D. Thomas, Phys. Rev. 116, 703 (1959).
27. J. M. Blatt and V. F. Weisskopf, Theoretical Nuclear Physics (John Wiley and Sons, New York, 1952).
28. A. G. W. Cameron, CRP-690, A. E. C. L. 433, 1958.
29. Y. Fujimoto and Y. Yamaguchi, Progr. Theoret. Phys. 5, 76 (1950).
30. W. J. Knox, A. R. Quinton, and C. E. Anderson (Sloane Physics Laboratory, Yale University), private communication.
31. M. M. Shapiro, Phys. Rev. 90, 171 (1953).
32. S. M. Polikanov and V. A. Druin, Soviet Physics - JETP 9, 522 (1959).
33. T. Sikkeland, G. E. Gordon, A. E. Larsh, J. R. Walton, and A. Ghiorso (Lawrence Radiation Laboratory), private communication.
34. A. Bohr, Kgl. Danske Videnskab. Selskab. Mat.-fys. Medd. 26, no. 14 (1952).
35. B. R. Mottelson and S. G. Nilsson, Kgl. Danske Videnskab. Selskab., Mat.-fys. Skr. 1, no. 8 (1959).
36. K. Alder, A. Bohr, T. Huus, B. Mottelson, and A. Winter, Revs. Modern Phys. 28, no. 4 (1956).
37. G. Breit, N. H. Hull, Jr., and R. L. Gluckstern, Phys. Rev. 87, 74 (1952).

38. Wladyslaw J. Swiatecki (Lawrence Radiation Laboratory), private communication.
39. Glen E. Gordon, Fission and Spallation in Nuclear Reactions Induced by Heavy Ions (Ph. D. thesis), UCRL-9083, May 1960.

This report was prepared as an account of Government sponsored work. Neither the United States, nor the Commission, nor any person acting on behalf of the Commission:

- A. Makes any warranty or representation, expressed or implied, with respect to the accuracy, completeness, or usefulness of the information contained in this report, or that the use of any information, apparatus, method, or process disclosed in this report may not infringe privately owned rights; or
- B. Assumes any liabilities with respect to the use of, or for damages resulting from the use of any information, apparatus, method, or process disclosed in this report.

As used in the above, "person acting on behalf of the Commission" includes any employee or contractor of the Commission, or employee of such contractor, to the extent that such employee or contractor of the Commission, or employee of such contractor prepares, disseminates, or provides access to, any information pursuant to his employment or contract with the Commission, or his employment with such contractor.

